processes

MDPI

Review

Graphene Oxide-Based Materials for the Remediation of Neurotoxic Organophosphates

Vladan Anićijević [1], Tatjana Mitrović [2], Tamara Terzić [3] and Tamara Lazarević-Pašti [3,*]

[1] Military Academy, University of Defence in Belgrade, Veljka Lukica Kurjaka 33, 11042 Belgrade, Serbia; anicijevicj.v@gmail.com
[2] Institute of Physics—National Institute of the Republic of Serbia, Pregrevica 118, 11000 Belgrade, Serbia; tmitrovic@ipb.ac.rs
[3] VINČA Institute of Nuclear Sciences—National Institute of the Republic of Serbia, University of Belgrade, Mike Petrovica Alasa 12–14, 11000 Belgrade, Serbia; tamara.tasic@vin.bg.ac.rs
* Correspondence: tamara@vin.bg.ac.rs

Abstract

Graphene oxide (GO), with its unique surface chemistry, adjustable oxidation degree, and large specific surface area, has emerged as a highly promising platform for environmental remediation. Among hazardous contaminants, organophosphates pose a significant global concern due to their persistence, high toxicity, and widespread presence in aquatic systems. This review provides a comprehensive overview of recent advances in the synthesis and functionalization of GO and GO-based composites specifically tailored for organophosphate removal. Particular emphasis is placed on strategies that optimize GO surface chemistry, defect engineering, and porosity control, which are critical determinants of adsorption efficiency and selectivity. In addition to its sorptive role, GO's role in photocatalytic and electrochemical degradation of organophosphates is discussed, demonstrating its multifunctionality as both an adsorbent and a catalytic support. Finally, challenges related to scalability, regeneration, and environmental safety of GO-based systems are examined, along with perspectives for future research aimed at developing sustainable, cost-effective, and environmentally friendly technologies to mitigate the risks associated with neurotoxic organophosphates.

Keywords: adsorption; photocatalysis; electrochemical degradation; environmental remediation; water pollution control

check for updates

Academic Editor: George Z. Kyzas

Received: 3 November 2025
Revised: 2 December 2025
Accepted: 10 December 2025
Published: 12 December 2025

Citation: Anićijević, V.; Mitrović, T.; Terzić, T.; Lazarević-Pašti, T. Graphene Oxide-Based Materials for the Remediation of Neurotoxic Organophosphates. *Processes* **2025**, *13*, 4028. https://doi.org/10.3390/pr13124028

Copyright: © 2025 by the authors. Licensee MDPI, Basel, Switzerland. This article is an open access article distributed under the terms and conditions of the Creative Commons Attribution (CC BY) license (https://creativecommons.org/licenses/by/4.0/).

1. Introduction

Organophosphates (OPs) constitute a large, structurally diverse class of phosphorus-containing compounds that have found use across multiple domains, including agriculture, medicine, industry, and defense. They have been applied as plasticizers [1], lubricating oil additives [2], flame retardants [3], and even as therapeutic agents in ophthalmology [4]. Still, their most prominent applications fall into two critical categories. The first is their extensive use as agricultural pesticides, where their high efficiency as insecticides has led to decades of global deployment [5]. The second, far more notorious, is their development as chemical warfare agents [6], commonly referred to as nerve agents (Figure 1).

The same biochemical principle that makes OPs highly effective insecticides also underlies their toxicity in humans and other non-target organisms. Their primary mode of action is the inhibition of acetylcholinesterase (AChE), the enzyme responsible for rapidly hydrolyzing the neurotransmitter acetylcholine in synaptic clefts [7]. By phosphorylating

the serine hydroxyl group in the active site of AChE, OPs irreversibly inactivate the enzyme, leading to the accumulation of acetylcholine at cholinergic synapses [8]. This overstimulation of muscarinic and nicotinic receptors disrupts neurotransmission throughout the central and peripheral nervous systems [9]. In insects, this manifests as rapid paralysis and death. In mammals, birds, aquatic organisms, and even beneficial insects, the outcome is equally harmful due to the non-selective nature of this mechanism. In humans, acute exposure to OPs can trigger a cholinergic crisis characterized by miosis, excessive salivation, muscle fasciculations, convulsions, respiratory distress, and, if untreated, death due to respiratory failure [10]. In contrast, chronic low-level exposure does not usually cause overt cholinergic symptoms but has been associated with subtle and long-term neurological outcomes. This phenomenon reflects the fact that chronic low-level exposure triggers subtle and sustained reductions in AChE activity, which can disrupt finely balanced neurophysiological processes that are highly sensitive to small perturbations. Over time, these mild but continuous disruptions interfere with homeostatic regulation of cholinergic signaling, leading to compensatory stress on neuronal networks, altered synaptic plasticity, dysregulated neuroendocrine responses, and increased vulnerability to neuroinflammatory and oxidative processes. Although not immediately life-threatening, such long-term disturbances can accumulate, ultimately resulting in premature or persistent neurological, cognitive, and affective impairments. Growing epidemiological and experimental evidence links such exposure to impaired cognitive performance [11], mood disorders including anxiety and depression [12], and an increased risk of neurodegenerative diseases such as Parkinson's [13] and Alzheimer's [14].

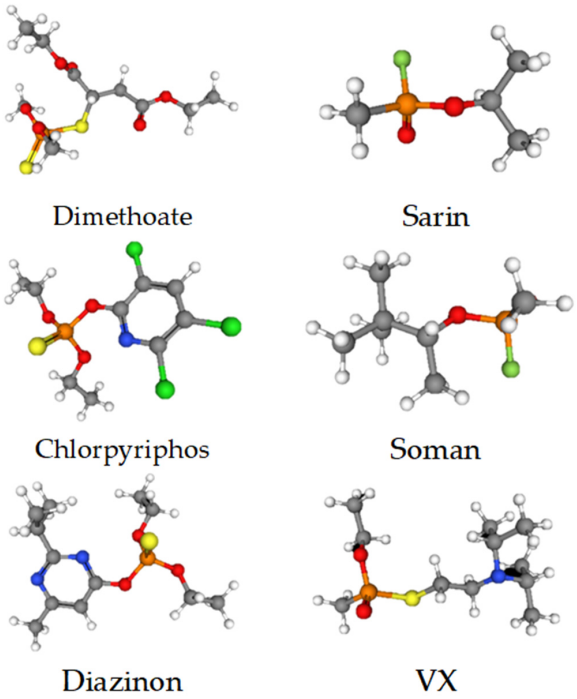


Figure 1. Structural formulas of selected organophosphate pesticides (**left**) and nerve agents (**right**). Atoms: grey—carbon, white—hydrogen, green—chlorine, blue—nitrogen, red—oxygen, orange—phosphorus, and yellow—sulfur.

Beyond their severe health effects, OPs are characterized by their persistence and mobility in the environment. Their residues are frequently detected in soil, food, and aquatic systems [15–17], raising global concerns about food safety, ecosystem stability, and human health. While regulatory limits vary across regions, available guidelines show that the required removal levels are quite strict. For example, the European Union Drinking

Water Directive sets a limit of 0.1 μg L^{-1} for any single pesticide and 0.5 μg L^{-1} for total pesticide residues [18], while the World Health Organization (WHO) and U.S. Environmental Protection Agency (US EPA) provide similar low-μg L^{-1} thresholds for several OPs [19,20]. Conventional treatment methods often suffer from limitations, including incomplete degradation, the generation of secondary waste, or a lack of selectivity [21–23]. Thus, there is a pressing need for advanced, sustainable technologies capable of efficiently removing and degrading OPs across diverse environmental matrices.

Graphene oxide (GO), a two-dimensional carbon nanomaterial, has attracted significant attention in recent years due to its unique combination of physicochemical properties. Structurally, GO consists of sp^2-hybridized carbon domains interspersed with sp^3 regions containing oxygenated functional groups such as hydroxyl, epoxy, and carboxyl moieties. In addition to these domains, GO also contains a significantly disrupted sp^2 network, where broken aromatic regions and defect sites strongly influence its reactivity, hydrophilicity, and surface interaction behavior [24]. This highly defective and chemically rich architecture provides GO with several advantages over pristine graphene, including enhanced hydrophilicity, improved colloidal stability in aqueous media, and a greater abundance of binding sites for contaminants [25]. Its large specific surface area [26] and adjustable degree of oxidation further enhance adsorption capacity. At the same time, the presence of functional groups allows facile modification and incorporation into composites with metals, metal oxides, polymers, and enzymes [25,27]. As a result, GO can act not only as a passive sorbent but also as an active support for catalytic, photocatalytic, or electrochemical degradation of toxic compounds [28]. These unique features have positioned GO and GO-based composites at the front of research in environmental remediation, with demonstrated efficiency against a broad spectrum of pollutants ranging from heavy metals [29] and dyes [30] to pharmaceuticals [31] and pesticides [32]. In the context of organophosphates, GO represents an emerging material of growing practical relevance, since its surface chemistry and high reactivity enable both strong adsorption and potential catalytic transformation of these neurotoxic compounds.

The aim of this review is to provide a comprehensive and focused overview of recent advances in the use of GO-based materials for the remediation of neurotoxic organophosphates. Although several reviews have examined GO for general water treatment, adsorption of organic pollutants, or photocatalytic degradation systems, these works typically address broad contaminant classes (e.g., dyes, pharmaceuticals, phenols, general pesticides) and rarely provide a critical synthesis tailored to organophosphate chemistry [33–37]. No available review integrates adsorption mechanisms with photocatalytic, electrochemical, and enzyme-assisted degradation routes specifically for OPs, nor do they bridge pesticide and chemical warfare agent simulant studies into a unified framework. The novelty of this work lies in consolidating these scattered findings into a single comparative perspective that links GO structure, OP molecular reactivity, and hybrid catalytic pathways. This paper will first outline the fundamental structural and chemical properties of GO relevant to contaminant removal. It will then summarize current strategies for modifying GO and its composites to enhance adsorption efficiency and selectivity toward organophosphates. Moreover, the paper will review developing approaches that integrate adsorption with catalytic pathways, including photocatalytic, electrochemical, and enzyme-assisted degradation. Finally, the review will address the key challenges of scalability, regeneration, and environmental safety, and highlight future perspectives for translating GO-based systems into sustainable and practical technologies that mitigate the risks posed by neurotoxic organophosphates.

2. Review Methodology

The literature search for this review was conducted between January and November 2025 using Web of Science, Scopus, PubMed, ScienceDirect, and Google Scholar. All available publication years were included to ensure complete coverage of both early foundational GO studies and recent developments. Search terms were adapted to each thematic section. They included combinations of: "graphene oxide", "GO composite", "rGO", "TiO_2-GO", "ZnO-GO", "organophosphate", "chlorpyrifos", "pesticide adsorption", "GO photocatalysis", "electro-Fenton GO", and related expressions. Studies were included if they reported experimental or computational results on GO or GO-based hybrids relevant to adsorption, photocatalysis, electrochemical degradation, or physicochemical interactions with organophosphate compounds. Papers where GO was not experimentally used or that focused on unrelated pollutants were excluded. Approximately 1800 records were initially retrieved, of which 186 met the relevance criteria after duplicate removal and title/abstract screening.

3. Properties of GO Relevant for Remediation

Understanding the fundamental properties of GO is essential for rationally designing and optimizing its performance in adsorption and catalytic remediation. The physicochemical behaviour of GO, defined by its atomic structure, surface functionality, and synthesis route, directly determines its reactivity, stability, and interactions with pollutants.

3.1. Structure, Synthesis, and Surface Chemistry of GO

GO is a two-dimensional carbon material obtained by the oxidation of graphite, followed by exfoliation, consisting of a hexagonal carbon lattice decorated with oxygen-containing functional groups. It serves as both a versatile adsorbent and a key precursor for reduced graphene derivatives used across technological and environmental applications [38–40]. Structurally, GO includes a carbon framework with disrupted sp^2 hybridization due to oxygen functionalities, producing a heterogeneous mixture of sp^2 and sp^3 domains that differentiate it from pristine graphene [38,41,42]. The most widely accepted structural model, proposed by Lerf and Klinowski based on ^{13}C NMR data, describes GO as consisting of aromatic "islands" separated by aliphatic regions bearing hydroxyl and epoxy groups [39,43,44]. These functional domains are randomly distributed, resulting in a rigid structure with increased interlayer spacing compared to graphite. Computational modeling further reveals that oxidation preferentially initiates at defect sites and propagates across basal planes, forming distinct oxidized and aromatic regions, in agreement with high-resolution microscopy [43].

GO was first synthesized by Brodie in 1859. However, modern production largely relies on modifications of the Hummer's method, developed in 1958, which remains the industrial standard. The process involves the oxidation of graphite using potassium permanganate ($KMnO_4$) in concentrated sulfuric acid (H_2SO_4) and sodium nitrate ($NaNO_3$) under controlled temperature conditions (initially 0–4 °C, followed by gradual heating) [45,46]. The reaction proceeds via the intercalation of acids, the formation of the active Mn_2O_7 species, and its subsequent thermal decomposition to yield atomic oxygen, which oxidizes the carbon lattice [45].

Several safer and more efficient modifications have since been proposed. The Tour method replaces $NaNO_3$ with a H_2SO_4/H_3PO_4 (9:1) mixture, reducing the evolution of toxic gases and achieving higher oxidation levels. Other environmentally improved protocols eliminate nitrates, employ alternative oxidants (e.g., H_3PO_4 or $Na_2B_4O_7{\cdot}10H_2O$), and adopt single-pot or shorter-duration processes [40,47–49]. Mechanistic studies confirm that Mn_2O_7 remains the key oxidizing intermediate, intercalating between graphite layers to

generate oxygen functionalities (epoxy, hydroxyl, carbonyl, and carboxyl) that define the reactivity and adsorption behaviour of GO. These oxygenated groups form the chemical foundation for the spectroscopic, electronic, and catalytic properties discussed in later sections. More recently, electrochemical synthesis has emerged as a greener, controllable alternative, relying on the anodic oxidation of graphite electrodes in mild electrolytes (such as ammonium sulfate or sodium nitrate). This method allows precise control of oxidation degree and flake size, avoids the use of concentrated acids, and produces GO with fewer metallic impurities, which is particularly beneficial for adsorption and electrochemical applications [50]. Complementary low-temperature oxidation routes, such as ozonation, UV/ozone treatment, sonication-assisted oxidation with mild oxidants, and plasma-assisted surface oxidation, are valuable for preparing thin films or partially oxidized graphene but are not widely used for bulk GO synthesis [38,51,52]. A schematic overview of the development of graphene oxide synthesis methods is presented in Figure 2. At the same time, detailed descriptions of the individual approaches, including their advantages and limitations, are summarized in Table 1.

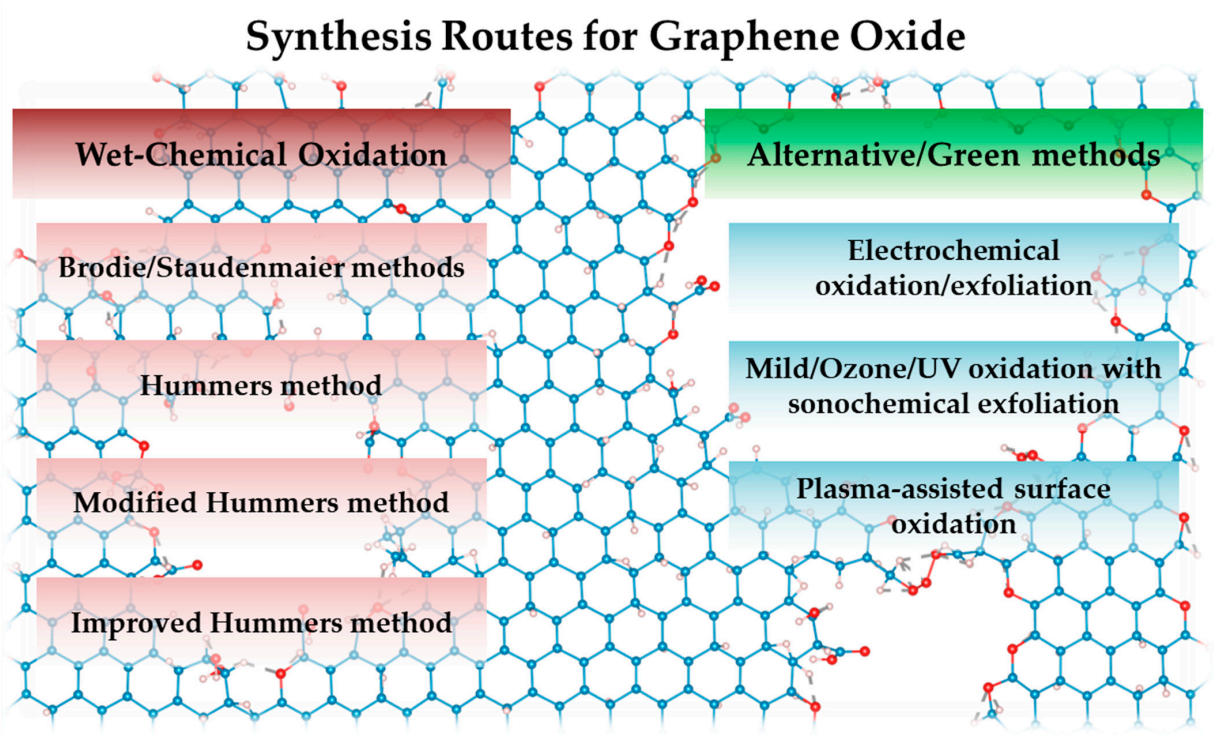


Figure 2. A schematic overview of the development of graphene oxide synthesis methods.

Table 1. Summary of graphene oxide synthesis methods.

Method	Key Chemicals/Tools	GO Quality	Advantages	Limitations
Hummers	$KMnO_4$, $NaNO_3$, H_2SO_4	Medium	Scalable, fast	Toxic NO_x (in original)
Improved/Modified Hummers	$KMnO_4$ + H_2SO_4/H_3PO_4	High	Safe, reproducible, large flakes	Requires acid handling
Brodie/Staudenmaier	$KClO_3$, HNO_3	High	High oxidation	Dangerous ClO_2 gas
Electrochemical	Electrolyte + power supply	Medium–High	Green, tunable	Smaller flakes
Ultrasonic/mild oxidation	H_2O_2, O_3	Low–Medium	Green	Low oxidation degree
Plasma/UV	O_2 plasma, O_3, UV	Surface only	Thin-film control	Not for bulk
Gas-phase/thermal	O_2, CO_2, NO_2	Low	Simple	Poor oxidation control

3.2. Physicochemical Characteristics and Structure-Property Relationships

GO exhibits a set of distinctive physicochemical features rising from its partially oxidized, mixed sp^2/sp^3 carbon framework. Interlayer spacing of dry graphene oxide is frequently determined using X-ray diffraction (XRD), as there is a characteristic reflection around $2\theta = 10^\circ$, which depends on the oxidation degree. This reflection actually originates from the (0002) reflection of graphite, which moves to a lower 2θ as the interlayer spacing increases to approximately 0.8 nm [53,54]. For example, in ref. [55] lower oxidation degree GO showed the reflection at $2\theta = 11.2^\circ$ (interlayer spacing of 0.789 nm), while a higher oxidation degree GO had the same reflection at $2\theta = 9.8^\circ$ (interlayer spacing of 0.902 nm). Trapped water can also affect the interlayer spacing, besides the oxidation degree. Atomic force microscopy (AFM) gives similar interlayer spacings of 0.7 to 0.8 nm when measured on well-defined few-layer GO samples [56,57]. It should be noted that the measurement method determines what we consider the interlayer spacing and the layer thickness. For example, in XRD, the interlayer spacing is obtained by analyzing reflections from the basal planes. In AFM, the thickness is defined through the atomic force field acting between the substrate, sample, and the AFM tip. The thickness of a single layer is the distance between the substrate and the AFM tip, divided by the number of GO layers in the analyzed GO sheet. On the other hand, the layer thickness could also be defined as the distance between the oxygen functional groups on the opposing sides of the basal plane. The layer thickness defined in this way can be calculated theoretically and ranges from 0.35 to 0.5 nm, depending on the types of groups that functionalize the basal plane [58]. Schematic representations of GO models are given in Figure 3. Individual sheets display lateral dimensions ranging from hundreds of nanometers to several micrometers and a characteristic wrinkled, paper-like morphology that contributes to their high specific surface area [38,41,59]. GO also shows characteristic optical properties, including a main absorption band at 230–233 nm (π-π^* transitions of C=C bonds) and a secondary band at 300–305 nm (n-π^* transitions of C=O bonds). The optical bandgap, typically between 2.5 and 3.6 eV, varies with the degree of oxidation, while broad photoluminescence originates from the distribution of oxygen functionalities [59,60].

A comprehensive understanding of GO's structure relies on a combination of advanced characterization techniques. X-ray Photoelectron Spectroscopy (XPS) enables quantitative determination of functional groups through C 1s and O 1s signal deconvolution, with asymmetric pseudo-Voigt fitting enhancing the accuracy of O/C ratio assessment [42,61]. Fourier Transform Infrared Spectroscopy (FTIR) reveals the characteristic vibrational modes of oxygen groups: O-H stretching (3200–3600 cm^{-1}), C=O stretching (1720 cm^{-1}), O-H bending of adsorbed water (1615 cm^{-1}), C-O-C stretching (1225 cm^{-1}), and C-O stretching (1056 cm^{-1}) [59]. Raman spectroscopy provides insight into structural disorder, revealing the D band (~1350 cm^{-1}) associated with sp^3 defects, the G band (~1590 cm^{-1}) originating from sp^2 carbon domains, and a weak 2D band related to layer stacking. The I_D/I_G ratio, typically 0.9–1.2 for GO compared to <0.1 for pristine graphene, quantifies the degree of structural disorder [41,59]. Thermogravimetric analysis (TGA) further complements this information by revealing decomposition stages corresponding to water loss (50–100 °C), decarboxylation (150–200 °C), lactone decomposition (200–300 °C), and oxidative carbon burn-off (530–620 °C) [62,63].

Standardized metrics further define high-quality GO as having an O/C ratio of 0.8–1.2, a sp^3 carbon fraction of 25–42% (by XPS), and an interlayer spacing of 0.7–0.8 nm [41]. The thermal stability of GO is strongly influenced by the synthesis route and atmosphere, with the decomposition onset shifting with oxidation degree, particle size, and residual metal ions; under inert atmospheres (N_2 or Ar), T_{max} values typically range from 558 °C to 616 °C [64].

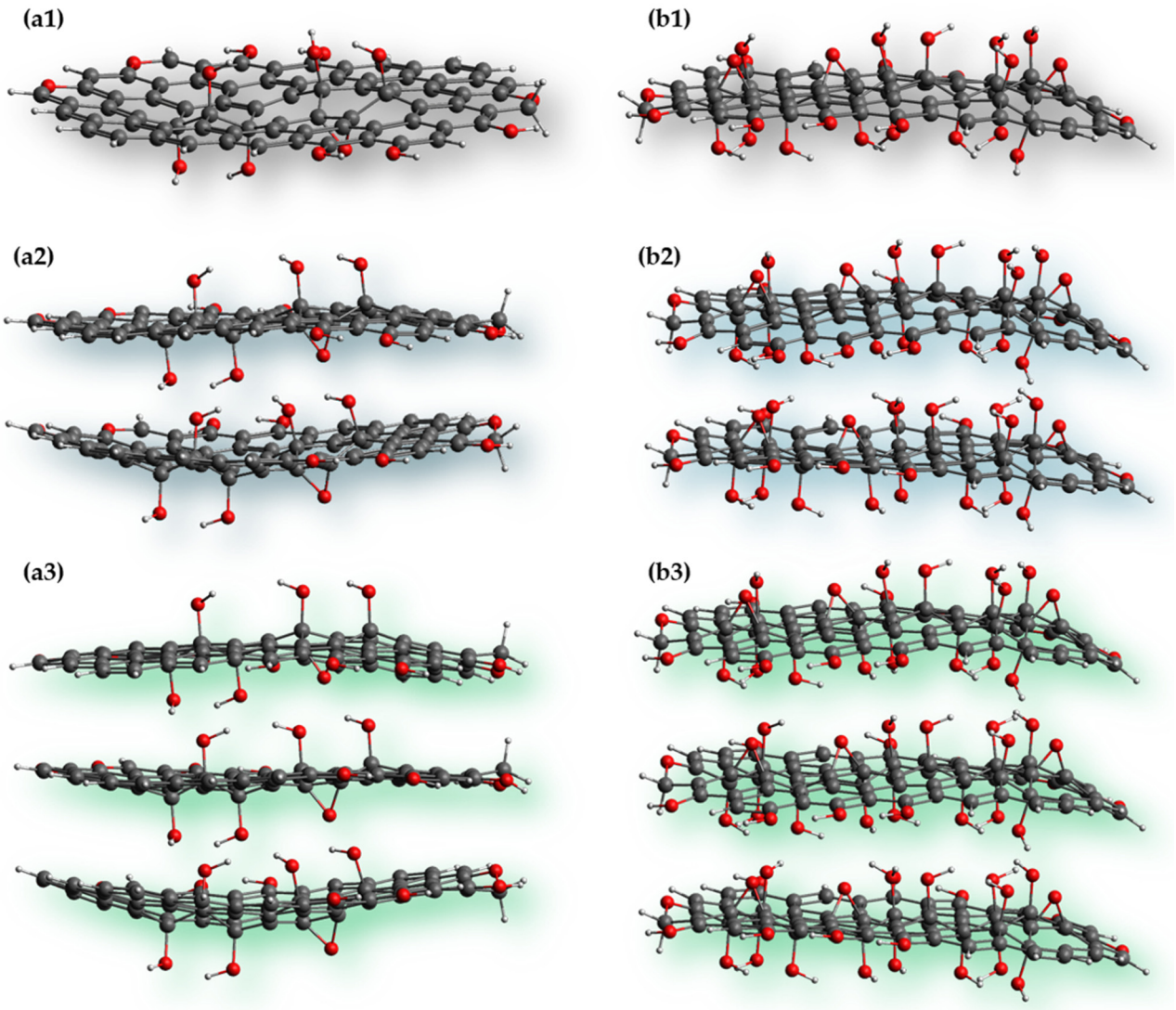


Figure 3. Models of GO with nominal composition (**a1**–**a3**) $C_{75}H_{25}O_{14}$ (C/O ratio 5.35) and (**b1**–**b3**) $C_{75}H_{34}O_{27}$ (C/O ratio 2.78), where single layer (**1**), bilayer (**2**), and trilayer (**3**) are presented. It can be seen that a higher oxidation degree ((**a1**) vs. (**b1**)) leads to greater basal-plane corrugation, while in both cases, layer stacking causes plane deformation. Also, a higher oxidation degree leads to larger interlayer spacing ((**a3**) vs. (**b3**)). The structures were optimized using semi-empirical quantum chemical calculations.

The macroscopic behaviour of GO is governed by three interconnected parameters: oxidation state, defect density, and lateral flake size. These variables together determine its electronic, mechanical, optical, and interfacial properties, and are key design parameters for remediation-oriented applications [65–67].

The oxidation state, as quantified by the C/O ratio, strongly influences electronic properties. Increasing oxidation disrupts the π-conjugated network, transforming GO from a semimetal to a wide-bandgap insulator [67–69]. Typical conductivity values range from $<10^{-6}$ S cm^{-1} at high oxidation (C/O~2–3) to ~10^{-2} S cm^{-1} at low oxidation (C/O > 10). Correspondingly, the optical bandgap narrows with decreasing oxidation, ranging from 2.5 eV to 3.6 eV [68,70]. Reduced GO (rGO) shows improved conductivity relative to oxidized GO due to partial restoration of the sp^2 network [67,71]. Defect density correlates closely with oxidation degree, but the relationship is non-linear. Graphite with higher initial defect density yields more efficiently oxidized GO [65,72]. Increased defects elevate I_D/I_G ratios and can induce paramagnetic behaviour [72,73]. Defects also modulate me-

chanical strength. Oxygen bridges and epoxide configurations locally stiffen the lattice, while random distributions act as stress concentrators. Optimal surface functionalization (~15–20%) retains significant tensile strength while preserving chemical activity [74,75].

Flake size plays an equally critical role. Larger GO sheets (>80 μm) provide enhanced mechanical strength and fatigue resistance in aerogels, whereas smaller flakes (<1 μm) improve interfacial compatibility in polymer composites but reduce bulk strength. Intermediate flake sizes (~5 μm) often yield an optimal balance between reinforcement and processability [76–79]. The size of the starting graphite strongly affects oxidation kinetics. Larger flakes require higher oxidant doses and harsher conditions, which can sometimes generate more defects [66,80]. Controlled sonication enables size reduction to ~100 nm while preserving C/O ratios and optical properties [80,81]. Dispersion and interfacial behaviour depend strongly on flake dimensions and functionalization. Smaller flakes exhibit higher critical coagulation concentrations (CCCs), implying better colloidal stability, while deprotonated edge carboxyls stabilize GO at alkaline pH. Ionic strength and counterion valence (Na^+ vs. Ca^{2+}) significantly alter aggregation behaviour [82,83]. Water structuring near GO surfaces follows a size-dependent pattern, with small flakes (<5 nm) inducing minimal dipole alignment, and larger ones (>7 nm) organizing structured hydration shells [82,84].

In practice, optimizing GO for composite or adsorption applications requires balancing conductivity, processability, and stability. Larger flakes favor load transfer and thermal transport, but small flakes enhance dispersion and surface accessibility. Similarly, higher oxidation improves hydrophilicity but compromises conductivity. Recognizing the need to balance competing parameters is essential for designing GO structures for targeted remediation performance [70,78,85,86].

3.3. Surface Area and Functional Groups Relevant to Organophosphate Interactions

The adsorption behaviour of GO toward organophosphate compounds is governed by the interaction between its large specific surface area and the abundance of surface functional groups [26]. The extended surface of GO provides a dense population of accessible adsorption sites, allowing multiple organophosphate molecules to interact simultaneously. Compared with bulk graphite, GO exhibits a markedly higher accessible area due to its exfoliated structure and interlayer spacing [87,88]. Nanostructured forms, such as GO/electrospun cellulose nanofiber composites, further enhance adsorption performance through expanded pore networks and interconnected fiber matrices that facilitate diffusion and molecular access [89].

Building on the structural insights discussed in Sections 3.1 and 3.2, the oxygenated functional groups distributed across the basal plane and sheet edges serve as active sites for hydrogen bonding, electrostatic attraction, and coordination with organophosphate species. These interactions strengthen surface affinity and, in some cases, promote partial catalytic hydrolysis of organophosphates under aqueous conditions.

The combination of a highly developed surface and diverse surface chemistry provides GO-based materials with large adsorption capacity and potential for molecular selectivity. While the high surface area favors physical uptake, oxygen functionalities contribute to specific interactions with phosphoryl and alkoxy groups. However, adsorption performance is not universal: aliphatic organophosphates such as dimethoate preferentially adsorb on oxidized, hydrophilic GO surfaces, whereas aromatic compounds like chlorpyrifos exhibit stronger affinity for more graphitic, π-conjugated carbons such as graphene nanoplatelets [54].

Together, these structural and chemical features define the possible roles of GO. Understanding how surface area and functionalization jointly influence organophosphate binding

is therefore essential for rational design of next-generation graphene-based sorbents for environmental remediation.

3.4. GO Among Carbon Allotropes

Carbon occurs in multiple allotropic forms, each defined by distinct hybridization states and structural dimensionalities. As mentioned, GO belongs to the two-dimensional (2D) family, in which carbon atoms are arranged in extended sheets of sp^2 and sp^3 domains. For context, carbon nanomaterials (CNMs) include four major dimensional categories (Figure 4): zero-dimensional (0D) species such as fullerenes, graphene quantum dots, and nanodiamonds; one-dimensional (1D) structures including carbon nanotubes and nanofibers; two-dimensional (2D) layers such as graphene, GO, and graphitic carbon nitride; and three-dimensional (3D) frameworks such as graphite, amorphous carbons, and porous activated carbons [90–92]. These allotropes differ fundamentally in bonding type, crystallinity, and accessible surface area, which together determine their suitability for adsorption and catalytic processes.

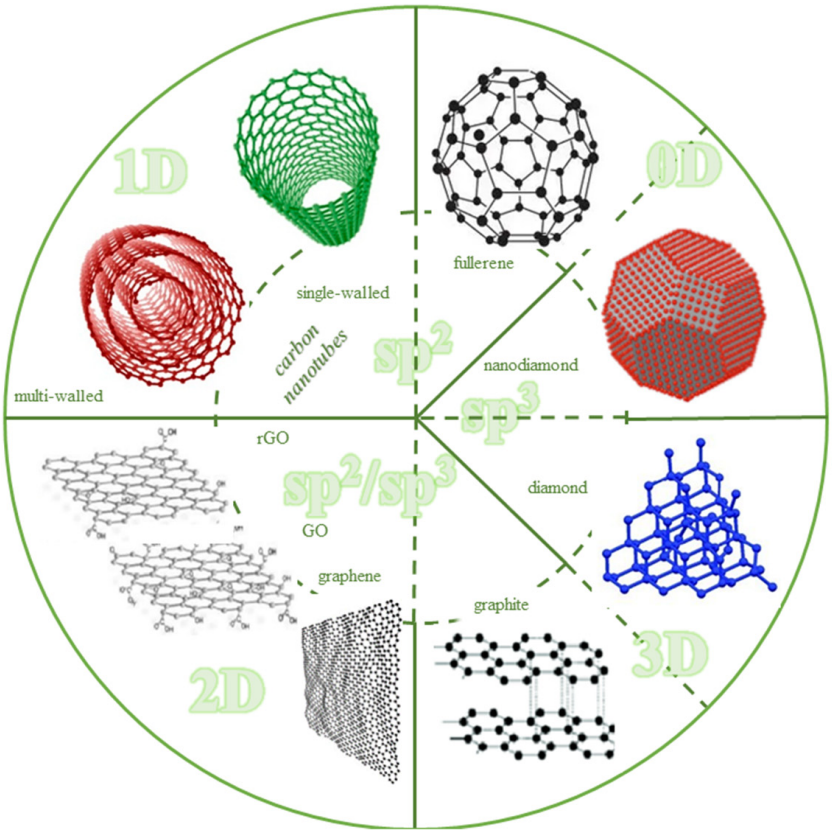


Figure 4. Classification of carbon materials.

Among crystalline forms, graphite is composed of stacked graphene layers bound by weak van der Waals interactions, giving it electrical conductivity within the basal planes and easy exfoliation into individual sheets. Diamond, by contrast, features sp^3-hybridized carbon atoms in a tetrahedral lattice, producing a dense, insulating, and mechanically robust structure. Amorphous carbons lack long-range order but often contain nanometer-scale graphitic or diamond-like domains, leading to moderate conductivity and tunable porosity [93]. A broad class of nanostructured carbons, including activated carbons, carbon aerogels, and carbonized biopolymers, can be observed as 3D porous networks composed of interconnected micro- and mesopores. Their internal surface area directs adsorption

capacity, and various physical or chemical activation routes are employed to enlarge pore volume and tailor surface chemistry [94–98].

Within this hierarchy, GO occupies a distinctive position. It couples the high theoretical surface area and mechanical integrity of graphene with abundant oxygenated functional groups that contribute to hydrophilicity, adjustable charge, and chemical reactivity. These features enable strong interfacial interactions with metal oxides, polymers, and organophosphate molecules, bridging the performance gap between inert graphitic carbons and conventional activated carbons. Therefore, GO combines structural order with the chemical diversity required for environmental remediation.

4. Adsorption of Organophosphates on GO-Based Materials

As discussed earlier, the adsorption of organophosphorus compounds on GO arises from a combination of physical and chemical interactions that collectively determine binding strength, selectivity, and reversibility. These interactions include hydrogen bonding, electrostatic attraction, π-π stacking, and coordination-type complexation, all of which depend on the surface chemistry of GO, pH, and the molecular features of the pesticide.

GO contains abundant oxygenated functional groups (hydroxyl, carboxyl, and epoxy) that act as both hydrogen bond donors and acceptors. Organophosphate molecules, characterized by a phosphoryl (P=O) and an alkoxy oxygen atom, readily participate in hydrogen bonding with these surface sites. Such interactions stabilize the adsorbed species and enhance surface wettability, allowing stronger physisorption on hydrophilic GO sheets [88,99]. Electrostatic attraction also contributes significantly, as the ionization of GO's acidic groups under neutral or mildly alkaline conditions imparts a negative surface charge, which interacts favourably with partially positively charged moieties on organophosphate molecules. The strength of this interaction depends strongly on solution pH and ionic strength. Adsorption is typically most effective around pH 4–6, where electrostatic attraction and hydrogen bonding coexist [88,100].

The sp^2-hybridized graphitic domains within GO retain π-conjugated regions capable of π-π stacking with aromatic or heterocyclic rings in organophosphate molecules (Figure 5). These interactions are particularly relevant for compounds containing benzene or phenyl substituents, where planar alignment of π systems produces additional stabilization energy and contributes to reversible adsorption [101–103]. In parallel, defect sites, vacancies, and oxygenated edges can form coordination-type or even partial covalent bonds with phosphorus centers or other electron-rich groups of organophosphates, leading to complexation. Such chemisorptive interactions are typically stronger and less reversible, often contributing to partial catalytic hydrolysis of P-O or P-S bonds. As a result, GO frequently acts as an adsorbent and also as a chemically active surface for organophosphate degradation [104,105].

A subtle yet important structural feature of GO is the presence of oxidative debris, small, highly oxidized polyaromatic fragments that adhere to its surface via π-π and hydrogen bonding. These fragments affect surface charge, hydrophilicity, and adsorption energetics, and their removal through alkaline washing can improve reproducibility and surface homogeneity [38,61]. Organophosphate adsorption on GO represents a continuum between physisorption and chemisorption, with the relative dominance of each mechanism determined by molecular structure, solution chemistry, and the extent of surface oxidation [89,100,102,103].

Experimental data consistently confirm that environmental conditions govern adsorption efficiency. pH exerts a critical influence by modulating both the GO surface charge and pesticide speciation. Under slightly acidic conditions, adsorption is typically maximized, whereas higher pH values increase surface deprotonation but diminish hydrogen

bonding, and strongly acidic environments lead to competition with protons. Temperature-dependent studies reveal spontaneous and exothermic adsorption behavior, with Gibbs free energy changes between −15 and −25 kJ mol^{-1} and negative enthalpy values indicative of exothermicity. Positive entropy changes further suggest increased randomness at the solid–liquid interface during adsorption [106,107]. Ionic strength also alters adsorption by screening electrostatic forces-high electrolyte concentrations reduce charge-based attraction but have minimal effect on π-π or van der Waals interactions [82,103].

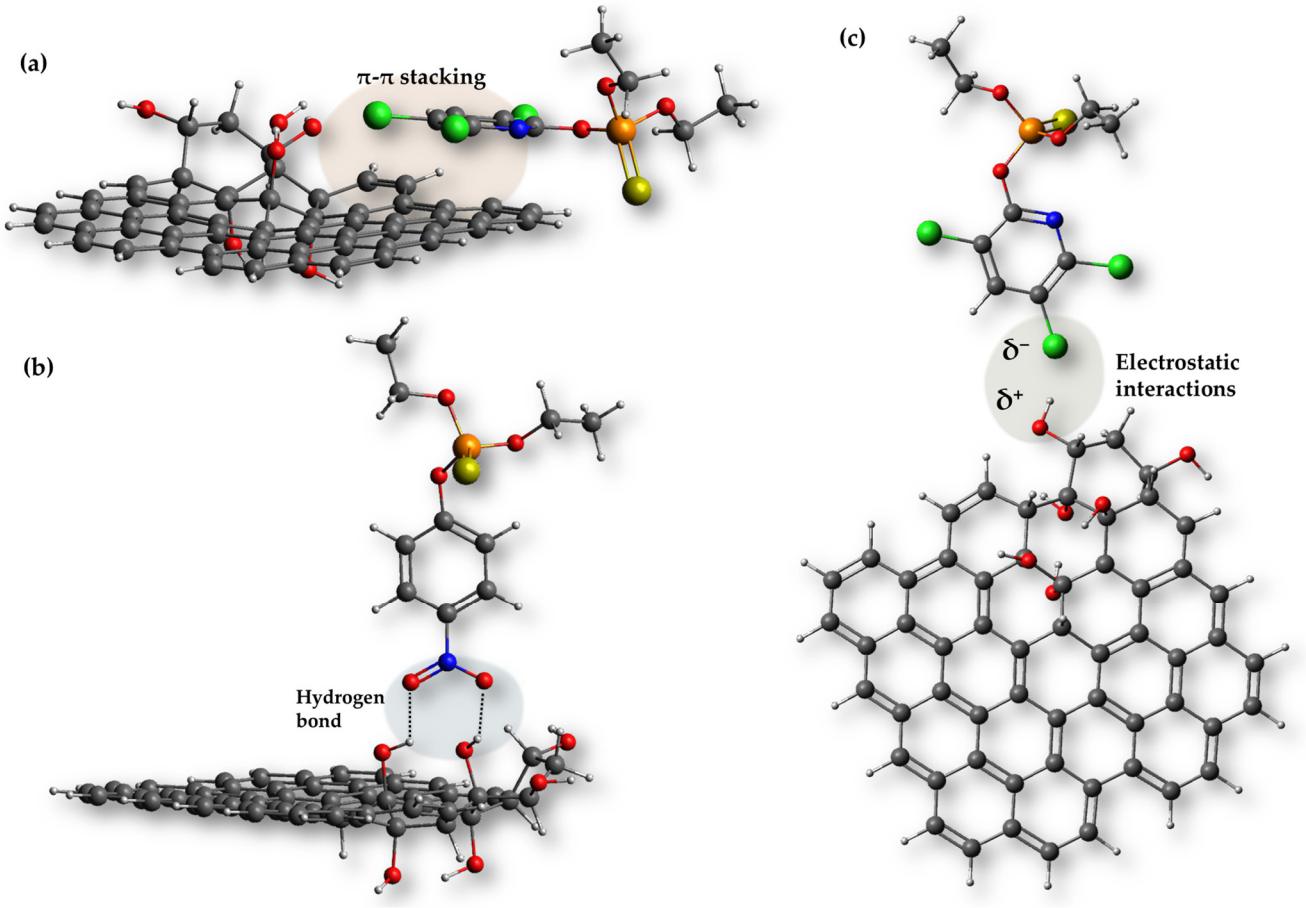


Figure 5. Examples of pesticides' interactions with carbon surfaces: (**a**) π-π stacking; (**b**) hydrogen bond; (**c**) electrostatic interactions. Atoms are color-coded as follows: grey—carbon, white—hydrogen, green—chlorine, blue—nitrogen, red—oxygen, orange—phosphorus, and yellow—sulfur.

Chemical functionalization of GO surfaces has proven highly effective in enhancing capacity and selectivity. Aminated GO introduces basic nitrogen groups that form strong electrostatic and hydrogen-bonding interactions with phosphoryl oxygens at near-neutral pH. Decoration with metal oxides such as Fe_3O_4, TiO_2, or ZnO allows coordination with phosphate oxygens. It can promote catalytic hydrolysis, while polymer coatings, particularly those based on chitosan or polyaniline, improve mechanical integrity and dispersion while supplying additional binding sites [104,105,108]. These hybrid systems often display higher adsorption capacities and better reusability, combining the advantages of physical and chemical sorption. Kinetic analyses further clarify these mechanistic differences. Adsorption of organophosphates on GO generally follows pseudo-second-order kinetics [89,107], implying that the rate-limiting step involves chemical interactions with surface sites, while pristine graphene exhibits pseudo-first-order kinetics characteristic of faster but weaker physisorption processes [109,110]. This distinction is summarized in Table 2, which highlights the contrasting kinetic regimes.

Table 2. Comparative kinetic behavior of GO and pristine graphene in organophosphate adsorption [89,107,109,110].

Parameter	Graphene Oxide	Pristine Graphene
Dominant kinetics	Pseudo-second-order	Pseudo-first-order
Adsorption rate	Slower (chemisorption)	Faster (physisorption)
R^2 values	0.994–0.999	0.92–0.98
Rate constant	10^{-3}–10^{-2} g mg^{-1} min^{-1}	10^{-2}–10^{-1} min^{-1}

Equilibrium data exhibit similar contrasts. Organophosphate adsorption on GO is typically well described by the Freundlich isotherm, indicative of a heterogeneous surface with multiple energy sites. In contrast, the Langmuir model better fits adsorption on pristine graphene, whose uniform aromatic surface promotes homogeneous monolayer coverage [54,89,106]. These distinctions are summarized in Table 3.

Table 3. Comparative equilibrium behaviour of GO and pristine graphene in organophosphate adsorption [54,89,106].

Model	Graphene Oxide	Pristine Graphene	Surface Character
Freundlich	Predominant ($R^2 > 0.95$)	Moderately applicable	Heterogeneous
Langmuir	Moderately applicable	Predominant ($R^2 > 0.95$)	Homogeneous

Across studies, GO shows markedly higher adsorption capacities, typically 50–200 mg g^{-1} compared to 20–80 mg g^{-1} for pristine graphene. They are attributed to its greater density of functional groups, higher hydrophilicity, and hybrid adsorption mechanisms [106,107,111,112]. These trends emphasize the dual role of GO as both an adsorptive and reactive interface, where physisorption ensures broad molecular uptake and chemisorption enables selective or catalytic binding. The chemical versatility and controllable surface chemistry of GO make it one of the most promising carbon-based materials for the removal of organophosphates from aqueous and environmental systems. Representative examples of GO-based adsorbents used for the removal of neurotoxic organophosphates are summarized in Table 4.

Table 4. GO-based adsorbents for the removal of neurotoxic organophosphates.

Type of GO-Based Material/Dose of Adsorbens	Type of Sample	Target Pollutant(s)/ Concentrations	Experimental Conditions (Matrix, pH, Temperature)	Adsorption Capacity (mg g^{-1})/Isotherm Model	Notable Features	Limitations	Reference
Fe_3O_4@SiO_2@GO-PEA nanocomposite/ 15 mg	Spiked aqueous samples, real environmental water samples (Vaal River and Vaal Dam, South Africa)	Chlorpyrifos, malathion, and parathion/1 µg/mL pesticide mix	10 mL water matrix, pH 7, 25 °C	11.1, 10.6, and 10.9, respectively/Sips model	Magnetic separation, fast kinetics, wide pH applicability, reusable for 10 cycles	Reduced magnetization, moderate capacity compared to some carbons	[111]
HPGA/2 mg	Air samples (synthetic air spiked with DMMP	Dimethyl methylphosphonate (DMMP)/ 0.5 mg L^{-1}	Dry air, room temperature	148	3D hierarchical porous aerogel, high SSA, excellent gas diffusion, ≥100 reuse cycles.	Requires thermal desorption, capacity depends on aerogel porosity	[113]
Activated carbon derived from sieve-like cellulose/GO composites (ACCE/G)/50 mg	Spiked aqueous samples (10 mL water)	Chlorpyrifos/ 2 mg L^{-1}	10 mL water, pH 1–7 tested (no strong pH 7, room temperature	152.5/Langmuir model	High porosity and surface area, reusable ≥8 cycles	Limitations: tested only in spiked water; requires organic solvent for regeneration; performance may vary with complex matrices	[106]

Table 4. *Cont.*

Type of GO-Based Material/Dose of Adsorbens	Type of Sample	Target Pollutant(s)/ Concentrations	Experimental Conditions (Matrix, pH, Temperature)	Adsorption Capacity (mg g^{-1})/Isotherm Model	Notable Features	Limitations	Reference
GO/ZIF-8 composite/20 mg	Spiked aqueous samples (10–50 mL water)	Chlorpyrifos and diazinon/ 1–10 mg L^{-1}	Water matrix, pH 7, 25 °C	103.72, and 90.17, respectively/Langmuir model	High porosity and GO/ZIF-8 synergy, stable, selective toward OPPs	/	[114]
GO/CNF/5 mg	Spiked aqueous samples, river and lake water, cabbage, rice	Methyl parathion, ethoprophos, sulfotepp, and chlorpyrifos/ 0.05–10 mg L^{-1}	Water or food-extract matrix	9.20, 3.44, 3.42 and 3.97, respectively/Langmuir model	Rapid adsorption (15 min)	/	[89]
Magnetic GO coated with polyvinyl alcohol (PVA@MGO nanocomposite)/ 15 mg	Apple juice and environmental water	Diazinon, fenitrothion, chlorpyrifos, profenofos, and ethion/ 10–120 mg L^{-1}	Food and water matrix, pH 6, 25 °C	161.29, 172.41, 217.39, 175.44, and 222.22, respectively/Langmuir model	Strong π-π and H-bond interactions, superparamagnetic, fast extraction (7 min), very low LODs (20–80 pg mL^{-1}).	Low selectivity toward different pesticide classes	[115]
rGO/0.0005–0.035 g	Spiked aqueous samples (Milli-Q water, 20 mL)	Phosmet/ 20–100 mg L^{-1}	Milli-Q water, pH 6.8, 15–45 °C	2680/Langmuir model	Very high capacity at low dose, exothermic adsorption	Strong dependence on adsorbent dose and temperature	[107]
Magnetic composite clay/GO/Fe_3O_4/ 1.14 g	Spiked aqueous samples (distilled/Milli-Q water)	Diazinon/ 1–5 mg L^{-1}	Distilled water, pH 6.9, 25.9 °C	7.384/Langmiur model	High adsorption efficiency (98.79%); fast kinetics, exothermic and spontaneous adsorption, reusable up to 20 cycles	Moderate capacity	[116]
Magnetic GO and carboxymethyl cellulose (MGOC) composite/ 0.4 g L^{-1}	Groundwater and polluted water	Chlorpyrifos/ 14 mg L^{-1}	Groundwater matrix, 20 °C	108.3/Langmuir model	Green, recyclable composite, strong chlorpyrifos affinity	/	[117]

5. Catalytic and Advanced Remediation Pathways

Effective remediation and removal of hazardous substances require understanding the specific chemical form in which a pollutant occurs, as a result of interconnected, microbiologically mediated processes, which are strongly determined by prevailing hydrogeochemical and redox conditions in water and soil environments [118–120].

5.1. Photocatalytic Degradation

GO has been extensively coupled with semiconductor photocatalysts to enhance light absorption, charge separation, and catalytic stability. Its oxygen-containing groups act as anchoring sites for nanoparticles, while the conjugated domains facilitate electron transport, thereby suppressing charge recombination. This synergy has enabled the design of numerous GO-based composites with high efficiency for degrading neurotoxic organophosphate pesticides [121] and warfare agent simulants [121,122] under UV or visible irradiation.

TiO_2-based systems are the most widely studied due to their robustness and cost-effectiveness. GO-TiO_2 nanocomposites have been demonstrated to remove dichlorvos and malathion from water [123], mineralize dichlorvos under visible light [124], and retain activity in real water matrices, such as treated wastewater and lake water [125]. Ultrasound-modified TiO_2/GO also exhibited bifunctional activity, combining adsorption and photocatalysis for the detoxification of warfare agent surrogates [126]. Other strategies involve ternary TiO_2 composites, such as TiO_2-rGO-MoS_2 hybrids, which achieve controllable performance depending on the MoS_2 loading [127]. Additionally, TiO_2 nanowires decorated with graphene quantum dots have been shown to double the degradation rates of pesticides compared to pristine TiO_2 [128]. Notably, TiO_2-rGO composites achieved nearly complete removal of sarin analogues, with efficiencies strongly dependent on rGO content [129].

ZnO-based composites are another important class, often chosen for their responsiveness to visible light. A GO-ZnO nanocomposite achieved 93.6% degradation of chlorpyrifos under sunlight within 90 min [130], while ZnO/rGO prepared hydrothermally showed a fourfold increase in photodegradation rates compared to bare ZnO due to improved charge transport [131]. Incorporating Co_3O_4 with ZnO/rGO further enhanced performance, achieving greater than 99% removal of parathion and diazinon [132].

Heterojunction and hybrid systems have expanded photocatalytic efficiency into the visible spectrum. WO_3-Fe_3O_4/rGO composites degraded diazinon with 94% efficiency in 100 min [133], while g-C_3N_4/GO/V_2O_5 catalysts removed more than 88% of chlorpyrifos in 120 min, with further improvement upon H_2O_2 addition [134]. GO/Fe_3O_4/CeO_2 heterojunctions demonstrated rapid charge transfer and efficient degradation of diazinon under visible light [135]. Similarly, innovative designs, such as GNP/ZrV_2O_7 reactors [136] or Pd–Fe_3O_4/GO nanoplates [137], have shown excellent performance. Meanwhile, amine-functionalized Fe_3O_4@GO composites have supported photo-Fenton activity against recalcitrant pesticides [138].

Table 5 provides an overview of key GO-based photocatalytic systems reported in the literature, illustrating how material design, the choice of semiconductor partner, and the light source collectively determine the degradation efficiency of organophosphate pollutants.

Table 5. Photocatalytic degradation of organophosphates using GO-based composites.

Composite System/Dose of Photocatalyst	Type of Sample	Target Pollutant(s)/ Concentration	Light Source	Degradation Efficiency/Kinetics	Notable Features	Limitations	Reference
TiO_2-rGO-MoS_2 ternary/1 g L^{-1}	Aqueous pesticide solution (laboratory-prepared)	Malathion/ 10 mg L^{-1}	UV/Vis	Tunable activity depending on MoS_2 loading	Improved electron-hole separation	Performance dependent on MoS_2 ratio, no toxicity or mineralization data	[127]
GO-ZnO nanocomposite/5–20 mg	Aqueous pesticide solution (laboratory-prepared)	Chlorpyrifos/10–40 ppm	Sunlight	93.6% in 90 min	Simple hydrothermal synthesis	Moderate surface area (2.99 m^2/g), decreased efficiency above 15 mg catalyst dose	[130]
GO-TiO_2/ 20–200 mg L^{-1}	Aqueous pesticide solution (laboratory-prepared)	Dichlorvos, malathion/0.5–20 mg L^{-1}	Visible	~90% removal, mineralization confirmed	Stable under multiple cycles	Real-water matrix not tested	[123]
GO-TiO_2/ 20–200 mg L^{-1}	Aqueous pesticide solution (laboratory-prepared)	Dichlorvos/0.5–20 mg L^{-1}	Visible	69% degradation, 64% mineralization	Stable performance	Real-water matrix not tested	[124]
GO-TiO_2 nanocomposite/60 mg L^{-1}	Distilled water, secondary treated wastewater, lake water	Dichlorvos, malathion	UV/Vis	~80% degradation after 80 min	Mineralization degree high, better performance vs. bare TiO_2, toxicity reduction assessed via Ellman assay	/	[125]
rGO-AgNP composite using *Curcubita maxima* extract/ 0.25–2.5 mg L^{-1}	Aqueous pesticide solution (laboratory-prepared)	Chlorpyrifos/200–5000 ppb	Sunlight	~75.5% degradation in 105 min	Green synthesis	Efficiency drops > 1 ppm, real-water matrix not tested	[139]
TiO_2/GO nanocomposite	Controlled atmosphere (in situ DRIFTS cell)	Dimethyl methylphosphonate/ 9.9 µg min^{-1}	Solar light	~80% degradation after 120 min	Enhanced photocatalytic activity due to GO	/	[140]
WO_3-Fe_3O_4/rGO composite/ 0.5–1.5 g L^{-1}	Aqueous pesticide solution (laboratory-prepared)	Diazinon/ 5–15 mg L^{-1}	Visible	94% degradation in 100 min	/	Real-water matrix not tested, performance decreases above 5 mg L^{-1}	[133]
rGO-Co_3O_4/ZnO NCs/ 10–120 mg L^{-1}	Aqueous pesticide solution (laboratory-prepared)	Parathion, diazinon/ 5–30 ppm	Visible	>99% in 140 min	Excellent recyclability	Real-water matrix not tested, no mineralization data	[132]
g-C_3N_4/GO/ V_2O_5	Aqueous pesticide solution (laboratory-prepared)	Chlorpyrifos	Visible	88–90% in 120 min	High stability over cycles	Real-water matrix not tested, no mineralization data	[134]

Table 5. *Cont.*

Composite System/Dose of Photocatalyst	Type of Sample	Target Pollutant(s)/ Concentration	Light Source	Degradation Efficiency/Kinetics	Notable Features	Limitations	Reference
GO/Fe_3O_4/CeO_2/ 10–40 mg	Aqueous pesticide solution (laboratory-prepared)	Diazinon/ 30 mg L^{-1}	Visible	97.9% in 60 min	Enhanced charge separation via CeO_2 functionalization	Real-water matrix not tested	[135]
GQDs/TiO_2 WT composite	Aqueous pesticide solution (laboratory-prepared)	Methiocarb, carbofuran, and dimethoate	Visible	2× faster than TiO_2 alone	Extended absorption range		[128]
rGO derived from bamboo leaves/ 10–25 mg L^{-1}	Aqueous pesticide solution (laboratory-prepared)	Monocrotophos/10–400 ppm	Visible	98% removal with a degradation rate of 0.036 ppm/min	Green synthesis	Real-water matrix not tested, no mineralization or toxicity data	[141]
SnS_2-Fe_3O_4/rGO/ 0.5 g L^{-1}	Aqueous pesticide solution (laboratory-prepared)	Diazinon/ 5 mg L^{-1}	Visible	~100% degradation in 40 min; TOC reduced 78%; pseudo-first-order kinetics	High catalytic performance and reusability	Real-water matrix not tested	[142]
ZnO/rGO nanocomposite/ 0.1–1 g L^{-1}	Aqueous pesticide solution (laboratory-prepared)	Dimethoate/ 5 mg L^{-1}	UV/Vis	Photodegradation rate 4× and efficiency 1.5× higher than bare ZnO; pseudo-first-order kinetics	/	Real-water matrix not tested	[131]
GO-Fe_3O_4/TiO_2/ 0.005–0.1 g	Aqueous pesticide solution (laboratory-prepared)	Chlorpyrifos/ 10 mg L^{-1}	Visible	97% degradation in 60 min	High photocatalytic activity and stability upon reuse	No TOC/mineralization data, real-water matrix not tested	[143]
GNPs/ZrV_2O_7	Aqueous pesticide solution (laboratory-prepared)	Chlorpyrifos/ 44.9 mg L^{-1}	Visible	~100% degradation in 60 min; pseudo-first-order kinetics	Innovative photocatalytic reactor design	Real-water matrix not tested, no mineralization or toxicity data	[136]
$CoFe_2O_4$@TiO_2/ rGO nanocomposite/ 0.05–0.6 g L^{-1}	Aqueous pesticide solution (laboratory-prepared)	Chlorpyrifos/ 5 mg L^{-1}	UV	High photocatalytic activity	Stable, recyclable, excellent catalytic activity	No TOC/mineralization data, real-water matrix not tested	[144]
TNP-Pd-Fe_3O_4/GO/30–80 mg	Aqueous pesticide solution (laboratory-prepared)	Parathion/ 10 mg L^{-1}	Visible	98.7% degradation		No TOC/mineralization data, real-water matrix not tested	[137]
AFG@MIL-101(Fe) (amine-functionalized Fe_3O_4@GO core–shell wrapped with MIL-101(Fe))	Aqueous pesticide solution (laboratory-prepared)	Diazinon, atrazine/30 ppm	Visible	~100% degradation of diazinon and 81% of atrazine in 105 min	Synergistic photo-Fenton and photocatalysis via GO-enhanced electron transfer	Real-water matrix not tested	[138]
Graphene/ZnO nanocomposite doped with Mn/ 50–200 mg L^{-1}	Aqueous pesticide solution (laboratory-prepared)	Diazinon/ 10 mg L^{-1}	UV	~100% removal after 60 min	Enhanced photocatalytic activity via Mn doping	Efficiency drops at >100 mg L^{-1} due to turbidity, no TOC or mineralization analysis, real-water matrix not tested	[145]
TiO_2-rGO composites	Gas-phase nerve agent simulant system	Sarin	UV	99.5% removal	Performance depends on rGO ratio	/	[129]

A growing number of studies demonstrate that coupling GO with metal oxides or magnetic nanoparticles can markedly enhance degradation pathways. The synergistic effects observed in these GO-semiconductor systems come primarily from GO's ability to act as an efficient electron mediator. Upon irradiation, photogenerated electrons in the semiconductor are rapidly transferred to GO, where they become delocalized across its sp^2 domains. This process suppresses electron-hole recombination, prolongs the lifetime of reactive species, and increases the rate of hydroxyl and superoxide radical formation [146–148]. In addition, the oxygenated functional groups and defect sites on GO promote interfacial charge transfer and provide additional adsorption sites for organophosphates, improving their local concentration at the catalytic interface. Still, the performance of these sys-

tems varies considerably depending on the target organophosphate, operational pH, and activation conditions. TiO_2-GO composites typically exhibit the highest photocatalytic degradation efficiencies under UV or simulated sunlight due to improved charge separation and an expanded absorption range [123–125,128]. Yet, their reusability is often limited by photocorrosion and the need for a light source. ZnO-GO systems exhibit comparable degradation rates at neutral pH and milder conditions but suffer from Zn^{2+} leaching over the long term, which compromises environmental compatibility [130,131,145]. Fe_3O_4-GO materials, although generally less active catalytically, offer unmatched magnetic recoverability and low operational cost, making them highly practical for large-volume treatment and repeated cycles [133,135,142].

These comparisons highlight a set of practical trade-offs:

- TiO_2-GO: highest photocatalytic efficiency, moderate cost, stability issues under prolonged illumination.
- ZnO-GO: effective under ambient/light conditions, inexpensive, but less durable.
- Fe_3O_4-GO: lower intrinsic activity but excellent recyclability and low-energy recovery.

GO-based photocatalytic composites have evolved from simple TiO_2 hybrids into sophisticated heterojunctions capable of visible-light activation, high degradation efficiency, and even partial mineralization of pesticide residues and simulants of warfare agents. Despite this progress, several critical challenges remain. The stability of catalytic performance in real environmental waters, where competing ions and organic matter interfere with active sites, remains a significant limitation to its practical applicability. Equally important are the issues of catalyst recovery and structural durability over repeated cycles. Moreover, balancing the growing complexity of synthesis routes with the need for cost-effective, scalable fabrication remains a significant challenge. Future research should focus on developing mechanistic models that explicitly link surface chemistry, light-harvesting dynamics, and degradation pathways. Bridging these knowledge and engineering gaps will ultimately determine whether GO-based photocatalysts can transition from laboratory demonstrations to real-world implementation in pesticide remediation.

5.2. Electrochemical Degradation

Beyond photocatalysis, graphene-based materials, particularly GO and its reduced form (rGO), have gained importance as efficient electrode modifiers in advanced electrochemical oxidation processes such as electro-Fenton (EF), electrochemical ozonation, and related hybrid systems. Their high conductivity, large surface area, and abundant functional groups promote in situ H_2O_2 generation and hydroxyl radical production, enabling rapid mineralization of organophosphate pesticides. Compared with conventional carbon electrodes, graphene-based systems offer superior electron transfer, chemical stability, and corrosion resistance, thereby directly translating into enhanced degradation efficiency [149]. The enhancement observed in GO-based EF and hybrid oxidation systems arises from several complementary roles played by GO. First, GO/rGO facilitate in situ H_2O_2 generation by accelerating the two-electron oxygen reduction pathway owing to their high conductivity and large density of electroactive surface sites [150]. Second, the oxygenated functional groups and edge defects on GO promote Fe^{2+}/Fe^{3+} redox cycling and thereby enhance •OH production from H_2O_2 [151]. Then, GO acts as an efficient electron-transfer mediator between the electrode and catalytic particles, reducing charge-transfer resistance and increasing current efficiency. Finally, when used as a support, GO prevents nanoparticle agglomeration and exposes a larger number of accessible catalytic sites [152,153].

Among various approaches, rGO-based electrodes have shown outstanding performance in EF systems. For instance, rGO-aminopyrazine-modified nickel foam achieved complete mineralization of dichlorvos, confirmed by stoichiometric release of chloride

and phosphate ions [154]. Nitrogen-doped GO and graphene composites containing Fe_3O_4/Fe_2O_3 further accelerated H_2O_2 activation, increasing EF efficiency and maintaining stability through multiple regeneration cycles [154]. Similarly, Fe_3O_4@N-GO heterojunction electrodes enabled complete degradation of dimethoate within 40 min, while mechanistic analysis confirmed hydrolysis and •OH-driven oxidation pathways [155]. Beyond binary systems, multi-component and doped electrodes have broadened the versatility of GO-based electrochemical materials. N-doped TiO_2/Graphene/Au and TiO_2/Graphene/Ag composites achieved nearly 100% diazinon removal through photo-electrocatalytic ozonation and retained high activity over seven successive cycles [156]. Hydrothermal rGO/V_2O_5 composites have also demonstrated efficient charge transfer and long-term stability [157]. These examples underscore the importance of rational heteroatom doping and metal incorporation in tuning both the catalytic and electrochemical behavior of GO electrodes.

In addition to remediation, graphene electrodes are also employed for the electrochemical detection of organophosphates, such as methyl parathion, either by direct reduction of nitro groups or via enzyme-inhibition-based sensing [158]. Such dual applicability highlights the multifunctional potential of GO-based systems in both environmental remediation and analytical monitoring.

Representative studies of electrochemical degradation using GO-based electrodes are summarized in Table 6, illustrating how electrode composition and architecture influence catalytic efficiency and operational stability.

Table 6. Electrochemical degradation of organophosphates using GO-based composites.

Electrode System	Type of Sample	Target Pollutant(s)/ Concentration	Process Type	Efficiency/Kinetics	Notable Features	Limitations	Reference
N-TiO_2/ Graphene/ Au (N-TiO_2/ G/Au)	Aqueous pesticide solution (laboratory-prepared)	Diazinon/ 10 mg L^{-1}	Photo-electrocatalysis/ photo-electrocatalytic ozonation	76.7% degradation in 60 min; ~100% with PEC ozonation	Enhanced degradation via PEC ozonation, stable for 7 cycles	Lower PEC efficiency without ozone, requires applied voltage (900 mV)	[156]
N-TiO_2/ Graphene/ Ag (N-TiO_2/ G/Ag)				81.1% degradation in 60 min; ~100% with PEC ozonation			
rGO-AmPyraz@3DNiF	Agricultural wastewater	Dichlorvos/50 mg L^{-1}	EF oxidation	100% degradation in 60 min	High H_2O_2 generation, stable and reusable, complete dichlorvos mineralization	Requires acidic pH	[154]
Bph-rGO	Aqueous pesticide solution (laboratory-prepared), wastewater matrix	Triclopyr/1 µM	Electrochemical oxidation	~60% removal	Enhanced charge storage, efficient oxidant generation, lower energy consumption	Phosphate buffer causes higher ohmic losses, performance drops in wastewater	[159]
hBN-rGO							
Fe_3O_4@N-GO	Simulated laboratory wastewater	Dimethoate/ 20 mg L^{-1}	Hetero EF	100% degradation in 40 min	N-doping enhanced conductivity and H_2O_2 generation, DFT confirmed P=S and P–O bond attack, reduced toxicity of by-products, excellent reusability		[155]

Electrochemical oxidation on graphene-modified electrodes typically follows pseudo-first-order kinetics, achieving near-complete removal of target pesticides. The reusability demonstrated across cycles confirms their mechanical robustness and chemical durability. Nonetheless, several obstacles remain, particularly electrode fouling, energy consumption, and the scalability of electrode fabrication. Future progress will depend on optimizing material durability, simplifying synthesis routes, and improving the energy efficiency of electrochemical systems to enable real-world applications in water treatment.

5.3. Enzyme-Assisted Remediation

In addition to physical and chemical pathways, enzymatic and biomimetic approaches have emerged as complementary routes for the degradation of organophosphates. GO and its derivatives have gained attention as versatile supports for enzyme-assisted degradation of organophosphates. The large surface area, π-π interactions, and abundance of oxygenated groups on GO provide an excellent platform for immobilizing hydrolytic enzymes such as phosphotriesterases (PTEs) and organophosphorus hydrolases (OPHs). Immobilization improves enzyme stability, reusability, and resistance to denaturation, while facilitating electron transfer in biosensing and degradation systems.

Early studies demonstrated that PTE and OPH enzymes immobilized on GO or rGO retained over 90% of their native activity and exhibited prolonged operational lifetimes. For instance, YT-PTE immobilized on rGO maintained up to 90% of its catalytic activity and enhanced electron transfer for paraoxon detection through the oxidation signal of p-nitrophenol, the hydrolysis product [160]. Noncovalent assembly of OPH nanocapsules onto GO similarly improved catalytic efficiency and reusability compared with the free enzyme [161,162].

In parallel with biological immobilization strategies, researchers have engineered enzyme-mimicking systems ("nanozymes") that reproduce the catalytic functions of OPH and PTE without requiring proteins. For example, Ma et al. [163,164] designed imidazole-rich polymer-GO hybrids and bimetallic Zn^{2+}/imidazole centres that mimic the active sites of natural hydrolases. These GO-based nanozymes achieved rapid hydrolysis of paraoxon and chlorpyrifos, with turnover frequencies up to 0.65 s^{-1} and retained more than 90% activity after several cycles. The catalytic activity arose from the synergistic interaction between imidazole clusters and surface carboxyl groups on GO, which facilitated nucleophilic attack on the phosphoester bond.

Recent developments have extended the concept of nanozyme-assisted remediation to hybrid materials combining GO with metal oxides and biopolymers. rGO/ZnO/chitosan composites, for instance, exhibited enhanced adsorption and catalytic degradation of diazinon following Freundlich-type isotherms, with optimal performance at neutral pH [165]. These multifunctional systems integrate adsorption, catalysis, and biocompatibility, suggesting potential for scalable and reusable pesticide treatment technologies.

Beyond environmental remediation, graphene-based enzymatic and nanozymatic systems are also being explored for the detection and detoxification of chemical warfare agents. Enzymes such as human serum paraoxonase 1 (PON1), phosphotriesterase (PTE), diisopropyl fluorophosphatase (DFPase), and related hydrolases have demonstrated notable activity against nerve agents by reactivating or replacing acetylcholinesterase [166]. These approaches illustrate the broader potential of GO-supported enzymatic systems at the interface of biosensing, catalysis, and defense.

While enzyme-assisted and biomimetic approaches offer high substrate specificity and mild reaction conditions, their large-scale implementation remains constrained by enzyme cost, sensitivity to environmental conditions, and the need for efficient immobilization and recovery strategies. Nevertheless, advances in GO-based hybrid materials and engineered nanozymes are rapidly bridging these gaps, offering promising routes toward sustainable and selective organophosphate remediation.

5.4. Multifunctionality of GO

A distinctive advantage of GO is its dual functionality: it can act as both a high-capacity adsorbent and a catalytic support. This property has inspired the development of multifunctional materials that integrate adsorption with photocatalytic, Fenton-like, or other advanced oxidation processes, achieving synergistic pollutant removal. Such systems

are particularly relevant for complex water matrices, where adsorption alone often fails to ensure complete detoxification.

The combination of GO with magnetic oxides enables simultaneous adsorption and catalytic degradation through photo- or electro-Fenton mechanisms. Magnetic GO composites have efficiently removed pesticides such as diazinon via coupled adsorption and photo-Fenton pathways [167]. Similarly, Fe_3O_4/GO nanocomposites activated persulfate to generate hydroxyl and sulfate radicals, leading to rapid pesticide oxidation [168]. Hybrid magnetic GO/ozonation systems (MGO/O_3) accelerated diazinon abatement compared with ozonation alone, confirming the dominant role of •OH radicals in synergistic degradation [169]. Graphene quantum dots (GQDs) decorated with Fe_3O_4 nanoparticles prepared from olive pomace also showed strong magnetic separability and high catalytic efficiency for malathion removal [170]. Similarly, bio-derived 3D magnetic GO composites synthesized from citrus peel via one-pot pyrolysis exhibited a hierarchical porous structure that enhanced both adsorption and radical-driven degradation [171].

Bio-derived GO-based hydrogels further expand the versatility of these systems by combining the biocompatibility of natural polymers with GO's catalytic and adsorptive properties. Xanthan gum-chitosan-GO hydrogels demonstrated efficient self-assembly and high sorption capacity, while chitosan/GQDs/Fe_3O_4 hydrogels achieved nearly 100% chlorpyrifos removal under ultrasonic assistance [172,173]. These materials are eco-friendly, reusable, and easily recoverable, highlighting their potential for sustainable water treatment.

GO has also been incorporated into mixed-matrix and thin-film nanocomposite membranes, which combine the advantages of polymeric flexibility with the reactivity of nanomaterials. These membranes exhibit improved permeability, selectivity, and antifouling properties, enabling continuous-flow operation and greater stability than traditional sorbents [174]. Recent designs also exploit GO's photothermal conversion capability. Graphene/UiO-66-NH_2 fabrics achieved ultrafast photothermal-assisted degradation of the nerve-agent simulant dimethyl-4-nitrophenyl phosphate (DMNP), halving its lifetime and maintaining >90% efficiency after five cycles [175]. 3D graphene aerogels and carbon-nanotube hybrids have demonstrated exceptional adsorption capacities for both pesticides and chemical warfare agents: hierarchical porous graphene aerogels efficiently trapped DMMP vapors [113], while CNT-reinforced graphene frameworks increased adsorption capacity by almost 40% compared to activated carbon [176].

Further innovations include combining GO with catalytic oxides and polyoxometalates. GO/MnO_2 nanocomposites enhanced the adsorption and degradation of organophosphate simulants DMMP and TEP [177], while Cu(OH)NO_3/GO composites accelerated organophosphate decomposition through improved electron transfer [178]. $Zr(OH)_4$/GO materials maintained catalytic activity for soman degradation even under humid conditions [179]. In parallel, emerging post-graphene 2D materials, such as transition-metal dichalcogenides and layered double hydroxides, are being investigated as next-generation analogues that combine large surface area with strong photocatalytic activity [180]. An especially promising direction involves mobile micro- and nanomotors that integrate GO or graphene derivatives with catalytic metals. ZrO_2-graphene/Pt tubular micromotors achieved 91% removal of methyl paraoxon within 5 min, demonstrating the feasibility of self-propelled, multifunctional cleanup systems [181].

Across these diverse configurations, a consistent trend emerges: integrating GO with catalytic, magnetic, or bio-based components yields synergistic systems capable of adsorption, degradation, and, in some cases, detection of organophosphate pollutants. The remaining challenges are primarily practical: ensuring reproducible synthesis, long-term stability, and cost-effective large-scale production. Nevertheless, multifunctional GO com-

posites represent one of the most promising directions toward integrated, sustainable, and adaptive remediation technologies capable of addressing complex contaminant mixtures.

6. Mechanistic Synthesis of GO-Based Pathways for OPs Removal

Mechanistic understanding of OPs removal by GO-based materials relies on a combination of spectroscopic, kinetic, and computational evidence. Across many studies, several conclusions are well supported, while others remain speculative. For instance, adsorption mechanisms are well supported by data. Several studies combining FTIR and XPS characterization with thermodynamic analysis have shown that OPs binding on GO-based adsorbents is typically dominated by hydrogen bonding and electrostatic interactions, with adsorption energies in the range characteristic of physisorption, although systems bearing strongly chelating nitrogen or metal sites can exhibit a measurable chemisorptive contribution [106,182]. The adsorption mechanisms proposed for GO-based materials are further supported by DFT and other computational simulations, which consistently show favorable adsorption energies and charge-transfer interactions between organophosphate molecules and oxygenated or graphitic domains of GO [54,88]. On the other hand, photocatalytic pathways are only partly supported. For TiO_2-GO and ZnO-GO hybrids, electron-hole separation is strongly supported by quenching, transient photocurrent measurements, and DFT-calculated charge transfer pathways [123,131]. However, proposed cleavage pathways for P-O and P-S bonds are often extrapolated and not always directly verified by intermediate detection (LC-MS), making mechanistic claims partially speculative.

7. Challenges and Limitations

Although GO-based nanomaterials have demonstrated remarkable efficiency in pollutant removal, their transition from laboratory studies to real-world implementation is constrained by stability, regeneration, scalability, and potential environmental risks.

7.1. Regeneration and Reusability

One of the most critical factors determining the practical applicability of GO-based materials is their ability to maintain performance over multiple operational cycles. A major challenge in applying GO-based photocatalysts and adsorbents on a large scale is ensuring long-term stability and regeneration efficiency without compromising activity. While several metal oxide-GO composites, such as CuO, ZnO, MgO, TiO_2, and WO_3-Fe_3O_4/rGO, demonstrate promising reusability and stable photocatalytic performance over multiple cycles [133,183], most studies remain limited to small-scale or batch tests. For instance, GQDs/TiO_2 nanotube composites retained approximately 80% of their photocatalytic efficiency after four cycles [128], and RMGO/Ag/V_2O_5 maintained over 80% degradation efficiency even after ten successive cycles [184], confirming excellent structural stability.

However, the regeneration of spent GO materials remains energy-intensive and often requires aggressive solvents or thermal treatment. Studies have shown that desorption and chemical regeneration (e.g., with HCl, NaOH, EDTA, or thiourea) can restore up to 95% of the adsorption capacity of metal-ion-loaded GO after several cycles [185–187]. Despite such successes, maintaining consistent catalytic activity after repeated use and preventing surface fouling remain unresolved. Furthermore, the tendency of GO sheets to restack during drying or regeneration reduces accessible surface area and active sites, limiting their practical reusability [188,189].

In recent years, several strategies have been proposed to mitigate the restacking of GO sheets during drying or regeneration. These include the introduction of polymeric or biopolymeric spacers, such as chitosan or cellulose nanofibers [190], to maintain interlayer separation, the formation of 3D aerogels and hydrogels that preserve porosity during sol-

vent removal [191,192], embedding metal oxide nanoparticles between GO layers to act as physical separators, and the use of mild drying techniques (freeze-drying, solvent exchange) to reduce capillary forces that drive sheet collapse [193]. While these approaches improve structural stability at the laboratory scale, their effectiveness under realistic operational and regeneration conditions remains largely unexplored.

7.2. Stability and Risk of Secondary Contamination

Ensuring material stability in natural and engineered water systems is another major concern. GO and its derivatives can aggregate or transform under variable pH, ionic strength, and natural organic matter content, affecting their performance and fate. Studies have shown that divalent cations such as Ca^{2+} and Mg^{2+} strongly promote GO aggregation via cross-linking of carboxyl groups, whereas negatively charged functional groups enhance colloidal stability in deionized water [185,194].

Despite good catalytic stability, GO's environmental persistence increases the risk of secondary contamination. When released into wastewater systems, GO has been found to disrupt microbial activity, reduce sludge dewaterability, and interfere with nutrient removal processes [189,195]. Moreover, its recovery by high-speed centrifugation is often impractical at industrial scales, leading to potential release of nanosheets into effluents. With anticipated increases in graphene production and recycling, it is essential to assess the long-term environmental behavior and potential bioaccumulation of GO-based materials. Although certain composites, such as RMGO/Ag/V_2O_5 or WO_3–Fe_3O_4/rGO, exhibit high stability across multiple cycles [133,184], the broader environmental safety concerns remain. Understanding the interactions between GO-based catalysts and natural organic matter, sediments, and microorganisms remains a prerequisite for the sustainable implementation of graphene-based catalysts [32,157].

7.3. Scalability and Synthesis Cost

Even with strong laboratory performance, cost and production scalability remain decisive factors for industrial translation. Despite exceptional performance at the laboratory scale, the mass production of high-quality GO and rGO remains costly and technically demanding. While chemical, thermal, and electrochemical reduction methods provide customizable properties, they often require toxic reagents or high-energy inputs [196]. Modified Hummers and improved chemical exfoliation routes have reduced environmental impact and enabled larger yields at lower costs [189]. To date, achieving uniform dispersion, controlled defect density, and consistent interfacial bonding in graphene–metal oxide composites remains a significant bottleneck [157]. Industrial synthesis methods such as chemical vapor deposition (CVD), epitaxial growth, and plasma-based techniques can deliver high-purity graphene but face scalability, reproducibility, and cost barriers [197,198]. Conversely, biomass-derived or hydrothermal routes offer eco-friendly alternatives but still require optimization of yield and quality. Techno-economic analyses remain scarce, and real cost comparisons with conventional adsorbents (e.g., activated carbon) are limited [188,189]. Future research must therefore focus on process simplification, renewable precursors, and integration of low-energy synthesis pathways to enhance both scalability and sustainability.

7.4. Ecotoxicity and Biocompatibility

Alongside technical concerns, the environmental and biological safety of graphene-based materials requires careful analysis. Graphene-based nanomaterials display remarkable physicochemical and electronic properties, yet their biocompatibility and ecotoxicity remain under debate. The same surface functionalities that provide high reactivity and adsorption capacity may also induce oxidative stress, membrane disruption, and genotoxic effects in living systems [199,200]. Studies indicate that GO exhibits higher reactivity than

pristine graphene or rGO due to its hydrophilicity and oxygenated groups, which can interact with cell membranes and microbial populations [201,202].

Toxicological investigations reveal dose- and size-dependent cytotoxicity. For instance, GO concentrations below 80 μg mL^{-1} typically show minimal effects, whereas higher doses lead to ROS generation and decreased cell viability [203–205]. Nonetheless, several studies have demonstrated the potential to tune surface chemistry to enhance biocompatibility. Green-synthesized rGO/AgNP composites have demonstrated strong antibacterial activity with reduced embryotoxicity [206], while plant-derived fluorescent GO structures have maintained over 80% cell viability in mammalian assays [207].

Overall, graphene-based nanomaterials can cross biological barriers such as the blood-brain and placental interfaces, and their fate in aquatic and terrestrial ecosystems remains poorly understood [196]. Therefore, comprehensive long-term studies on transformation, bioaccumulation, and chronic effects are crucial before GO-based technologies can be safely implemented on a large scale.

8. Future Perspectives

Future progress in the application of GO-based nanomaterials for organophosphate remediation will depend on translating current laboratory advances into adaptive, field-ready technologies that address both civilian and defense needs. The next generation of GO-based systems is expected to evolve into smart hybrid composites that integrate multiple functionalities, combining the conductivity and tunable surface chemistry of GO with the catalytic efficiency of metals, the selectivity of enzymes, and the flexibility of polymers. Rationally designed GO-metal-enzyme-polymer hybrids could unite adsorption, catalysis, and biodegradation within a single self-regenerating structure, capable of continuous operation under dynamic environmental conditions.

A central goal in future research is to enhance molecular recognition and selectivity toward structurally diverse organophosphates, including both agricultural pesticides and chemical warfare agents. Advances in heteroatom doping, enzyme-mimetic surface design, and electronic-structure engineering can enable fine control over catalytic sites that selectively target the P-O and P-S bonds characteristic of these compounds. Coupling experimental design with computational modeling and machine-learning-driven screening may accelerate the discovery of GO-based materials with tailored degradation pathways and predictable activity across complex organophosphate mixtures.

Realistic testing environments remain a crucial missing link. While most studies focus on model compounds in deionized water, the next phase must address the fluctuations in pH, ionic strength, and natural organic matter found in actual wastewater, soil leachates, and contaminated groundwater. Integrating GO-based catalysts into filtration membranes, soil-treatment amendments, and modular photoreactors can bridge the gap between controlled laboratory studies and field-scale implementation. Such validation is crucial for emergency response scenarios, agricultural runoff control, and chemical defense operations. In parallel, GO-based nanomaterials offer promising opportunities for rapid-response decontamination systems. Their high conductivity, mechanical strength, and catalytic activity make them ideal for miniaturized electrochemical or photocatalytic modules capable of on-site neutralization of organophosphate pesticides and nerve-agent simulants. Portable devices based on GO electrodes or fabrics could be deployed for real-time detoxification and monitoring in both military and civilian contexts, providing an integrated approach to chemical threat mitigation. Equally important is ensuring that this technological progress aligns with sustainability principles. The future of GO-based remediation lies in adopting green synthesis routes, such as biomass-derived graphene, solvent-free exfoliation, and recyclable catalysts, combined with comprehensive life-cycle assessments. Embedding these

innovations within circular-economy frameworks can minimize environmental burdens while maximizing societal benefits.

GO thus occupies a key position at the interface of environmental chemistry, materials science, and defense technology. Its evolution from a laboratory nanomaterial to a multifunctional, deployable platform could redefine how humanity responds to both chronic pollution and acute chemical threats. By uniting advanced material design, computational optimization, and sustainable manufacturing, GO-based systems have the potential to become the cornerstone of next-generation strategies for the selective, efficient, and eco-responsible remediation of pesticides and chemical warfare agents alike.

9. Conclusions

GO and its derivatives have emerged as one of the most adaptable materials for addressing complex environmental and chemical challenges. Their surface functionality, high reactivity, and compatibility with diverse functional components have enabled the creation of advanced composites capable of adsorption, catalytic degradation, and selective remediation of both organophosphate pesticides and warfare agents. The recent evolution of GO-based systems toward hybrid and multifunctional platforms underlines their potential to connect environmental chemistry, materials science, and chemical defence. Despite these advances, translating GO-based technologies from the laboratory to large-scale applications remains at an early stage. Long-term stability, regeneration efficiency, ecotoxicity, and economic feasibility continue to define the boundaries of practical implementation. Overcoming these challenges will require not only improvements in material design and green synthesis but also standardized testing in realistic environmental conditions.

Looking ahead, future progress will depend on how effectively GO can be incorporated into practical and sustainable technologies such as catalytic filters, hybrid membranes, and portable devices for decontamination and sensing, including rapid-response systems for neurotoxic organophosphate pesticides and related chemical warfare agents. Achieving this vision will require closer integration between fundamental materials research and applied environmental engineering, guided by transparent risk assessment and sustainability criteria. When guided by sustainability principles and responsible innovation, GO has the potential to transform how we address chemical contamination, linking scientific progress, environmental protection, and human safety.

Author Contributions: Conceptualization, T.L.-P.; methodology, T.T., T.M., V.A. and T.L.-P.; validation, T.L.-P.; investigation, T.T., T.M., V.A. and T.L.-P.; resources, T.L.-P.; data curation, T.T., T.M., V.A. and T.L.-P.; writing—original draft preparation, T.T., T.M., V.A. and T.L.-P.; writing—review and editing, T.L.-P.; visualization, V.A.; supervision, T.L.-P.; project administration, T.L.-P.; funding acquisition, T.L.-P. All authors have read and agreed to the published version of the manuscript.

Funding: T.L.-P. and T.T. acknowledge the support provided by the Serbian Ministry of Science, Technological Development and Innovations (contract number: 451-03-136/2025-03/200017). V.A. acknowledges the support provided by the Serbian Ministry of Defence, Republic of Serbia (project name: Research on influence of characteristics of explosive ordnance on safety in Ministry of Defense and Army of Serbia, project code: VA-TT/1/22-24). T.M. acknowledges the support provided by Serbian Ministry of Science, Technological Development and Innovations (contract number: 0801–116/1). T.T. acknowledges the support provided by the Serbian Academy of Sciences and Arts (project no. F-49).

Data Availability Statement: No new data were created or analyzed in this study. Data sharing is not applicable to this article.

Acknowledgments: The authors acknowledge Igor A. Pašti for help with generating the GO structures presented in Figure 3, using semi-empirical quantum chemical calculations as implemented in MOPAC.

Conflicts of Interest: The authors declare no conflicts of interest.

References

1. Yin, S.; den Ouden, F.; Cleys, P.; Klimowska, A.; Bombeke, J.; Poma, G.; Covaci, A. Personal environmental exposure to plasticizers and organophosphate flame retardants using silicone wristbands and urine: Patterns, comparisons, and correlations. *Sci. Total Environ.* **2024**, *927*, 172187. [CrossRef] [PubMed]
2. Dao, T.L.K.; Tieu, A.K.; Tran, B.H. Comprehensive Investigation of Various Organophosphate Intercalated CoAl-LDHs As Additives in Polyalphaolefin. *ACS Appl. Eng. Mater.* **2024**, *2*, 10–23. [CrossRef]
3. Macan Schönleben, A.; den Ouden, F.; Yin, S.; Fransen, E.; Bosschaerts, S.; Andjelkovic, M.; Rehman, N.; van Nuijs, A.L.N.; Covaci, A.; Poma, G. Organophosphorus Flame Retardant, Phthalate, and Alternative Plasticizer Contamination in Novel Plant-Based Food: A Food Safety Investigation. *Environ. Sci. Technol.* **2025**, *59*, 9209–9220. [CrossRef]
4. Furman, B.L. Echothiophate☆. In *Reference Module in Biomedical Sciences*; Elsevier: Amsterdam, The Netherlands, 2018. [CrossRef]
5. Lazarević-Pašti, T.; Milanković, V.; Tasić, T.; Petrović, S.; Leskovac, A. With or Without You?—A Critical Review on Pesticides in Food. *Foods* **2025**, *14*, 1128. [CrossRef]
6. Anićijević, V.a.K.R. Organophosphates as Chemical Warfare Agents. In *Organophosphates: Detection, Exposure and Occurrence. Volume 2: Acute Exposure and Treatments*; NOVA Science Publisher: Hauppauge, NY, USA, 2022; Volume 2.
7. Silman, I.; Sussman, J.L. Acetylcholinesterase: 'classical' and 'non-classical' functions and pharmacology. *Curr. Opin. Pharmacol.* **2005**, *5*, 293–302. [CrossRef]
8. Colović, M.B.; Krstić, D.Z.; Lazarević-Pašti, T.D.; Bondžić, A.M.; Vasić, V.M. Acetylcholinesterase inhibitors: Pharmacology and toxicology. *Curr. Neuropharmacol.* **2013**, *11*, 315–335. [CrossRef] [PubMed]
9. Aroniadou-Anderjaska, V.; Figueiredo, T.H.; de Araujo Furtado, M.; Pidoplichko, V.I.; Braga, M.F.M. Mechanisms of Organophosphate Toxicity and the Role of Acetylcholinesterase Inhibition. *Toxics* **2023**, *11*, 866. [CrossRef] [PubMed]
10. Bereda, G. Acute Cardiac Arrhythmias in Organophosphate Poisoning: From Bradycardia to Atrial Fibrillation. *Indian J. Clin. Cardiol.* **2025**, *6*, 398–404. [CrossRef]
11. Arida, R.; Elkader, H.-T.A.A.; Aborajeh, S.; Helmy, M.M.; El-Mallah, A.I.; Abdallah, S.M.; El-Yazbi, A.F. Prolonged Exposure to Organophosphates Worsens the Cognitive Outcome of Prediabetes: Possible Modulation by Arachidonic Acid Supplementation. *J. Pharmacol. Exp. Ther.* **2024**, *389*, 506. [CrossRef]
12. Suarez-Lopez, J.R.; Hood, N.; Suárez-Torres, J.; Gahagan, S.; Gunnar, M.R.; López-Paredes, D. Associations of acetylcholinesterase activity with depression and anxiety symptoms among adolescents growing up near pesticide spray sites. *Int. J. Hyg. Environ. Health* **2019**, *222*, 981–990. [CrossRef]
13. Samareh, A.; Pourghadamyari, H.; Nemtollahi, M.H.; Ebrahimi Meimand, H.A.; Norouzmahani, M.E.; Asadikaram, G. Pesticide Exposure and Its Association with Parkinson's Disease: A Case–Control Analysis. *Cell. Mol. Neurobiol.* **2024**, *44*, 73. [CrossRef]
14. Voorhees, J.R.; Remy, M.T.; Erickson, C.M.; Dutca, L.M.; Brat, D.J.; Pieper, A.A. Occupational-like organophosphate exposure disrupts microglia and accelerates deficits in a rat model of Alzheimer's disease. *npj Aging Mech. Dis.* **2019**, *5*, 3. [CrossRef]
15. Ore, O.T.; Adeola, A.O.; Bayode, A.A.; Adedipe, D.T.; Nomngongo, P.N. Organophosphate pesticide residues in environmental and biological matrices: Occurrence, distribution and potential remedial approaches. *Environ. Chem. Ecotoxicol.* **2023**, *5*, 9–23. [CrossRef]
16. López-Benítez, A.; Guevara-Lara, A.; Domínguez-Crespo, M.A.; Andraca-Adame, J.A.; Torres-Huerta, A.M. Concentrations of Organochlorine, Organophosphorus, and Pyrethroid Pesticides in Rivers Worldwide (2014–2024): A Review. *Sustainability* **2024**, *16*, 8066. [CrossRef]
17. Tesi, G.O.; Okpara, K.E.; Tesi, J.N.; Agbozu, I.E.; Techato, K. Assessment of organophosphate pesticides in soils and vegetables from agricultural areas of Delta Central District, Nigeria. *Sci. Rep.* **2025**, *15*, 8267. [CrossRef]
18. Available online: https://eur-lex.europa.eu/eli/dir/2020/2184/oj (accessed on 25 September 2025).
19. Available online: https://www.who.int/publications/i/item/9789241549950 (accessed on 25 September 2025).
20. Available online: https://www.epa.gov/ground-water-and-drinking-water/national-primary-drinking-water-regulations (accessed on 25 September 2025).
21. Li, W.; Zhan, H.; Dong, C.; Wu, S.; Mulcahy, D.; Duan, J. Detoxication of organophosphate pesticides in source waters by incorporation of an alkaline hydrolysis procedure in conventional drinking water treatment processes. *J. Water Process Eng.* **2023**, *53*, 103917. [CrossRef]
22. Nandhini, A.R.; Harshiny, M.; Gummadi, S.N. Chlorpyrifos in environment and food: A critical review of detection methods and degradation pathways. *Environ. Sci. Process. Impacts* **2021**, *23*, 1255–1277. [CrossRef]

23. Ragnarsdottir, K.V. Environmental fate and toxicology of organophosphate pesticides. *J. Geol. Soc.* **2000**, *157*, 859–876. [CrossRef]
24. Zheng, X.; Zhai, R.; Zhang, Z.; Zhang, B.; Liu, J.; Razaq, A.; Ahmad, M.A.; Raza, R.; Saleem, M.; Rizwan, S.; et al. Graphene-Oxide-Based Fluoro- and Chromo-Genic Materials and Their Applications. *Molecules* **2022**, *27*, 2018. [CrossRef] [PubMed]
25. Mushahary, N.; Sarkar, A.; Basumatary, F.; Brahma, S.; Das, B.; Basumatary, S. Recent developments on graphene oxide and its composite materials: From fundamentals to applications in biodiesel synthesis, adsorption, photocatalysis, supercapacitors, sensors and antimicrobial activity. *Results Surf. Interfaces* **2024**, *15*, 100225. [CrossRef]
26. Zhang, S.; Wang, H.; Liu, J.; Bao, C. Measuring the specific surface area of monolayer graphene oxide in water. *Mater. Lett.* **2020**, *261*, 127098. [CrossRef]
27. Huang, X.; Zhao, W.; Khalilov, F.; Xu, N. Graphene Oxide: Preparation and Medical Research. *Materials* **2025**, *18*, 2855. [CrossRef]
28. Jun, B.-M.; Nam, S.-N.; Jung, B.; Choi, J.S.; Park, C.M.; Choong, C.E.; Jang, M.; Jho, E.H.; Son, A.; Yoon, Y. Photocatalytic and electrocatalytic degradation of bisphenol A in the presence of graphene/graphene oxide-based nanocatalysts: A review. *Chemosphere* **2024**, *356*, 141941. [CrossRef]
29. Pandey, G.; Rajput, N.S.; Sharma, U.K.; Chauhan, M.S.; Lamba, N.P. Remediation of environmental issues using graphene based materials for water purification: Synthesis, kinetics, and factors effecting the removal of heavy metal ions. *Next Mater.* **2025**, *8*, 100765. [CrossRef]
30. Goyat, R.; Saharan, Y.; Singh, J.; Umar, A.; Akbar, S. Synthesis of Graphene-Based Nanocomposites for Environmental Remediation Applications: A Review. *Molecules* **2022**, *27*, 6433. [CrossRef] [PubMed]
31. Rameshwar, S.S.; Rajamohan, N. Magnetic graphene based materials for removal of pharmaceutical compounds—Review on applications and machine learning approaches. *J. Mol. Struct.* **2025**, *1328*, 141309. [CrossRef]
32. Gupta, T.; Ratandeep; Dutt, M.; Kaur, B.; Punia, S.; Sharma, S.; Sahu, P.K.; Pooja; Saya, L. Graphene-based nanomaterials as potential candidates for environmental mitigation of pesticides. *Talanta* **2024**, *272*, 125748. [CrossRef]
33. Thakur, S.; Bi, A.; Mahmood, S.; Samriti; Ruzimuradov, O.; Gupta, R.; Cho, J.; Prakash, J. Graphene oxide as an emerging sole adsorbent and photocatalyst: Chemistry of synthesis and tailoring properties for removal of emerging contaminants. *Chemosphere* **2024**, *352*, 141483. [CrossRef]
34. Madduri, S.B.; Kommalapati, R.R. Harnessing Novel Reduced Graphene Oxide-Based Aerogel for Efficient Organic Contaminant and Heavy Metal Removal in Aqueous Environments. *Nanomaterials* **2024**, *14*, 1708. [CrossRef]
35. Zubair, M.; Roopesh, M.S.; Ullah, A. Challenges and prospects: Graphene oxide-based materials for water remediation including metal ions and organic pollutants. *Environ. Sci. Nano* **2024**, *11*, 3693–3720. [CrossRef]
36. Anegbe, B.; Ifijen, I.H.; Maliki, M.; Uwidia, I.E.; Aigbodion, A.I. Graphene oxide synthesis and applications in emerging contaminant removal: A comprehensive review. *Environ. Sci. Eur.* **2024**, *36*, 15. [CrossRef]
37. Thakur, K.; Kandasubramanian, B. Graphene and Graphene Oxide-Based Composites for Removal of Organic Pollutants: A Review. *J. Chem. Eng. Data* **2019**, *64*, 833–867. [CrossRef]
38. Jiříčková, A.; Jankovský, O.; Sofer, Z.; Sedmidubský, D. Synthesis and Applications of Graphene Oxide. *Materials* **2022**, *15*, 920. [CrossRef] [PubMed]
39. He, H.; Klinowski, J.; Forster, M.; Lerf, A. A new structural model for graphite oxide. *Chem. Phys. Lett.* **1998**, *287*, 53–56. [CrossRef]
40. Nishina, Y. Mass Production of Graphene Oxide Beyond the Laboratory: Bridging the Gap Between Academic Research and Industry. *ACS Nano* **2024**, *18*, 33264–33275. [CrossRef] [PubMed]
41. Donato, K.Z.; Tan, H.L.; Marangoni, V.S.; Martins, M.V.S.; Ng, P.R.; Costa, M.C.F.; Jain, P.; Lee, S.J.; Koon, G.K.W.; Donato, R.K.; et al. Graphene oxide classification and standardization. *Sci. Rep.* **2023**, *13*, 6064. [CrossRef] [PubMed]
42. Kovtun, A.; Jones, D.; Dell'Elce, S.; Treossi, E.; Liscio, A.; Palermo, V. Accurate chemical analysis of oxygenated graphene-based materials using X-ray photoelectron spectroscopy. *Carbon* **2019**, *143*, 268–275. [CrossRef]
43. Sinclair, R.C.; Coveney, P.V. Modeling Nanostructure in Graphene Oxide: Inhomogeneity and the Percolation Threshold. *J. Chem. Inf. Model.* **2019**, *59*, 2741–2745. [CrossRef]
44. Siklitskaya, A.; Gacka, E.; Larowska-Zarych, D.; Malolepszy, A.; Mazurkiewicz, M.; Stobinski, L.; Marciniak, B.; Lewandowska-Andralojc, A.; Kubas, A. Lerf–Klinowski-type models of graphene oxide and reduced graphene oxide are robust in analyzing non-covalent functionalization with porphyrins. *Sci. Rep.* **2021**, *11*, 7977. [CrossRef]
45. Chen, X.; Qu, Z.; Liu, Z.; Ren, G. Mechanism of Oxidization of Graphite to Graphene Oxide by the Hummers Method. *ACS Omega* **2022**, *7*, 23503–23510. [CrossRef]
46. Syed, N.; Sharma, N.; Kumar, L. Synthesis of Graphene Oxide (GO) by Modified Hummers Method and Its Thermal Reduction to Obtain Reduced Graphene Oxide (rGO)*. *Graphene* **2017**, *6*, 1–18. [CrossRef]
47. Méndez-Lozano, N.; Pérez-Reynoso, F.; González-Gutiérrez, C. Eco-Friendly Approach for Graphene Oxide Synthesis by Modified Hummers Method. *Materials* **2022**, *15*, 7228. [CrossRef]
48. Zaaba, N.I.; Foo, K.L.; Hashim, U.; Tan, S.J.; Liu, W.-W.; Voon, C.H. Synthesis of Graphene Oxide using Modified Hummers Method: Solvent Influence. *Procedia Eng.* **2017**, *184*, 469–477. [CrossRef]
49. Korucu, H. Optimization of Graphene Oxide Synthesis Using Hummers Method. *Gazi Univ. J. Sci.* **2024**, *37*, 1132–1152. [CrossRef]

50. Yu, Q.; Wei, L.; Yang, X.; Wang, C.; Chen, J.; Du, H.; Shen, W.; Kang, F.; Huang, Z.-H. Electrochemical synthesis of graphene oxide from graphite flakes exfoliated at room temperature. *Appl. Surf. Sci.* **2022**, *598*, 153788. [CrossRef]
51. Cheng, Y.C.; Kaloni, T.P.; Zhu, Z.Y.; Schwingenschlögl, U. Oxidation of graphene in ozone under ultraviolet light. *Appl. Phys. Lett.* **2012**, *101*, 073110. [CrossRef]
52. Magro, M.R.; Vella, D.A.; Cassar, G. Synthesis of graphene oxide: A refined approach. *Carbon Trends* **2025**, *20*, 100509. [CrossRef]
53. Lyu, J.; Wen, X.; Kumar, U.; You, Y.; Chen, V.; Joshi, R.K. Separation and purification using GO and r-GO membranes. *RSC Adv.* **2018**, *8*, 23130–23151. [CrossRef] [PubMed]
54. Lazarević-Pašti, T.; Anićijević, V.; Baljozović, M.; Anićijević, D.V.; Gutić, S.; Vasić, V.; Skorodumova, N.V.; Pašti, I.A. The impact of the structure of graphene-based materials on the removal of organophosphorus pesticides from water. *Environ. Sci. Nano* **2018**, *5*, 1482–1494. [CrossRef]
55. Krishnamoorthy, K.; Veerapandian, M.; Yun, K.; Kim, S.J. The chemical and structural analysis of graphene oxide with different degrees of oxidation. *Carbon* **2013**, *53*, 38–49. [CrossRef]
56. Romero, M.P.; Marangoni, V.S.; de Faria, C.G.; Leite, I.S.; Silva, C.d.C.C.e.; Maroneze, C.M.; Pereira-da-Silva, M.A.; Bagnato, V.S.; Inada, N.M. Graphene Oxide Mediated Broad-Spectrum Antibacterial Based on Bimodal Action of Photodynamic and Photothermal Effects. *Front. Microbiol.* **2020**, *10*, 2019. [CrossRef]
57. Sun, X.; Luo, D.; Liu, J.; Evans, D.G. Monodisperse chemically modified graphene obtained by density gradient ultracentrifugal rate separation. *ACS Nano* **2010**, *4*, 3381–3389. [CrossRef]
58. Dobrota, A.S.; Pašti, I.A.; Mentus, S.V.; Skorodumova, N.V. A DFT study of the interplay between dopants and oxygen functional groups over the graphene basal plane—Implications in energy-related applications. *Phys. Chem. Chem. Phys.* **2017**, *19*, 8530–8540. [CrossRef]
59. Khalili, D. Graphene oxide: A promising carbocatalyst for the regioselective thiocyanation of aromatic amines, phenols, anisols and enolizable ketones by hydrogen peroxide/KSCN in water. *New J. Chem.* **2016**, *40*, 2547–2553. [CrossRef]
60. Vekhande, H.N.; Bagawade, J.A. Synthesis and characterization of graphene oxide using a modified Hummers method for enhanced quality and yield. *Fuller. Nanotub. Carbon Nanostruct* **2025**, 1–7. [CrossRef]
61. Aliyev, E.; Filiz, V.; Khan, M.M.; Lee, Y.J.; Abetz, C.; Abetz, V. Structural Characterization of Graphene Oxide: Surface Functional Groups and Fractionated Oxidative Debris. *Nanomaterials* **2019**, *9*, 1180. [CrossRef] [PubMed]
62. Yap, P.L.; Farivar, F.; Jämting, Å.K.; Coleman, V.A.; Gnaniah, S.; Mansfield, E.; Pu, C.; Landi, S.M.; David, M.V.; Flahaut, E.; et al. International Interlaboratory Comparison of Thermogravimetric Analysis of Graphene-Related Two-Dimensional Materials. *Anal. Chem.* **2023**, *95*, 5176–5186. [CrossRef] [PubMed]
63. Farivar, F.; Lay Yap, P.; Karunagaran, R.U.; Losic, D. Thermogravimetric Analysis (TGA) of Graphene Materials: Effect of Particle Size of Graphene, Graphene Oxide and Graphite on Thermal Parameters. *C* **2021**, *7*, 41. [CrossRef]
64. Ajala, O.J.; Tijani, J.O.; Bankole, M.T.; Abdulkareem, A.S. A critical review on graphene oxide nanostructured material: Properties, Synthesis, characterization and application in water and wastewater treatment. *Environ. Nanotechnol. Monit. Manag.* **2022**, *18*, 100673. [CrossRef]
65. Mohanta, Z.; Gaonkar, S.K.; Kumar, M.; Saini, J.; Tiwari, V.; Srivastava, C.; Atreya, H.S. Influence of Oxidation Degree of Graphene Oxide on Its Nuclear Relaxivity and Contrast in MRI. *ACS Omega* **2020**, *5*, 22131–22139. [CrossRef]
66. Benzait, Z.; Trabzon, L. Graphite Size Effect on Chemical Expansion and Graphene Oxide Properties. *ACS Omega* **2022**, *7*, 37885–37895. [CrossRef]
67. Morimoto, N.; Kubo, T.; Nishina, Y. Tailoring the Oxygen Content of Graphite and Reduced Graphene Oxide for Specific Applications. *Sci. Rep.* **2016**, *6*, 21715. [CrossRef] [PubMed]
68. Aldosari, H. The Effect of Carbon/Oxygen Ratio upon Structure-Property Relationships in Polymer/Graphene Nanocomposites. *Nano Hybrids Compos.* **2022**, *37*, 59–78. [CrossRef]
69. Khanmamedova, E. Electrical conductivity properties of graphene oxide. *Sci. Collect. «InterConf+»* **2023**, *32*, 594–598. [CrossRef]
70. Chi, H.; Zhao, M.; Li, Y.; Guo, Y.; Liu, B.; Yue, G.; Miao, Y.; Li, N.; Wang, H. Size-Dependent Photoelectric Properties of Graphene Oxide for a Phosphorescent Green Organic Light-Emitting Diode Achieving a High Device Efficiency. *ACS Appl. Nano Mater.* **2025**, *8*, 1925–1934. [CrossRef]
71. Fajardo, S.; Ocón, P.; Arranz, A.; Rodríguez, J.L.; Pastor, E. MnO_2-modified ZIF-67 supported on doped reduced graphene oxide as highly active catalyst for the oxygen reduction reaction. *J. Catal.* **2024**, *432*, 115448. [CrossRef]
72. Mohanta, Z.; Atreya, H.S.; Srivastava, C. Correlation between defect density in mechanically milled graphite and total oxygen content of graphene oxide produced from oxidizing the milled graphite. *Sci. Rep.* **2018**, *8*, 15773. [CrossRef]
73. Ćirić, L.; Sienkiewicz, A.; Djokić, D.M.; Smajda, R.; Magrez, A.; Kaspar, T.; Nesper, R.; Forró, L. Size dependence of the magnetic response of graphite oxide and graphene flakes—An electron spin resonance study. *Phys. Status Solidi (B)* **2010**, *247*, 2958–2961. [CrossRef]
74. Nasr Esfahani, M.; Shahbeigi, S.; Jabbari, M. Effect of oxygen configurations on the mechanical properties of graphene oxide. *J. Appl. Phys.* **2022**, *132*, 174302. [CrossRef]

75. Sharma, B.B.; Kedare, A.; Muralidharan, G.; Govind Rajan, A. Understanding the Effects of Surface and Edge Functionalization on the Mechanical Properties of Graphene and Graphene Oxide. *ChemPhysChem* **2025**, *26*, e202400919. [CrossRef]
76. Gao, W.; Zhao, N.; Yao, W.; Xu, Z.; Bai, H.; Gao, C. Effect of flake size on the mechanical properties of graphene aerogels prepared by freeze casting. *RSC Adv.* **2017**, *7*, 33600–33605. [CrossRef]
77. Wu, X.; Lin, T.F.; Tang, Z.H.; Guo, B.C.; Huang, G.S. Natural rubber/graphene oxide composites: Effect of sheet size on mechanical properties and strain-induced crystallization behavior. *Express Polym. Lett.* **2015**, *9*, 672–685. [CrossRef]
78. Belmonte, D.; Mella, C.; Sánchez-Sanhueza, G.; Opazo-Capurro, A.; Aguilar-Bolados, H.; Boury, B.; Urbano, B.F. Impact of graphene oxide lateral dimensions on the properties of methacrylated gelatin nanocomposite hydrogels. *J. Mater. Chem. B* **2023**, *11*, 1987–1997. [CrossRef]
79. Yang, Z.; Wang, L.; Li, J.; Shi, Z.; Wang, M.; Sheng, J.; Fei, W. Lateral size effect of reduced graphene oxide on properties of copper matrix composites. *Mater. Sci. Eng. A* **2021**, *820*, 141579. [CrossRef]
80. Méndez-Romero, U.A.; Pérez-García, S.A.; Fan, Q.; Wang, E.; Licea-Jiménez, L. Lateral size reduction of graphene oxide preserving its electronic properties and chemical functionality. *RSC Adv.* **2020**, *10*, 29432–29440. [CrossRef]
81. Coleman, B.R.; Knight, T.; Gies, V.; Jakubek, Z.J.; Zou, S. Manipulation and Quantification of Graphene Oxide Flake Size: Photoluminescence and Cytotoxicity. *ACS Appl. Mater. Interfaces* **2017**, *9*, 28911–28921. [CrossRef] [PubMed]
82. Suter, J.L.; Coveney, P.V. Principles governing control of aggregation and dispersion of aqueous graphene oxide. *Sci. Rep.* **2021**, *11*, 22460. [CrossRef] [PubMed]
83. Szabo, T.; Maroni, P.; Szilagyi, I. Size-dependent aggregation of graphene oxide. *Carbon* **2020**, *160*, 145–155. [CrossRef]
84. Peng, E.; Todorova, N.; Yarovsky, I. Effects of Size and Functionalization on the Structure and Properties of Graphene Oxide Nanoflakes: An in Silico Investigation. *ACS Omega* **2018**, *3*, 11497–11503. [CrossRef]
85. Ma, J.; Dai, S.; Guo, Z.; Shang, L.; Ao, Y.; Jin, L. Impact of graphene oxide lateral sizes on the mechanical and thermal properties of carbon fiber composites. *Polym. Compos.* **2025**, *46*, 2061–2072. [CrossRef]
86. Ji, Z.; Dervishi, E.; Doorn, S.K.; Sykora, M. Size-Dependent Electronic Properties of Uniform Ensembles of Strongly Confined Graphene Quantum Dots. *J. Phys. Chem. Lett.* **2019**, *10*, 953–959. [CrossRef] [PubMed]
87. Shi, X.; Cheng, C.; Peng, F.; Hou, W.; Lin, X.; Wang, X. Adsorption properties of graphene materials for pesticides: Structure effect. *J. Mol. Liq.* **2022**, *364*, 119967. [CrossRef]
88. Tadawattana, P.; Kawashima, K.; Sittiwanichai, S.; T-Thienprasert, J.; Mori, T.; Pongprayoon, P. Exploring the Capabilities of Nanosized Graphene Oxide as a Pesticide Nanosorbent: Simulation Studies. *ACS Omega* **2025**, *10*, 8951–8959. [CrossRef]
89. Aris, N.I.F.; Rahman, N.A.; Wahid, M.H.; Yahaya, N.; Abdul Keyon, A.S.; Kamaruzaman, S. Superhydrophilic graphene oxide/electrospun cellulose nanofibre for efficient adsorption of organophosphorus pesticides from environmental samples. *R. Soc. Open Sci.* **2020**, *7*, 192050. [CrossRef] [PubMed]
90. Lazarević-Pašti, T. Carbon Materials for Organophosphate Pesticide Sensing. *Chemosensors* **2023**, *11*, 93. [CrossRef]
91. Kroto, H.W.; Heath, J.R.; O'Brien, S.C.; Curl, R.F.; Smalley, R.E. C60: Buckminsterfullerene. *Nature* **1985**, *318*, 162–163. [CrossRef]
92. Belenkov, E.A.; Greshnyakov, V.A. Classification schemes for carbon phases and nanostructures. *New Carbon Mater.* **2013**, *28*, 273–282. [CrossRef]
93. Ajayan, P.M. Nanotubes from Carbon. *Chem. Rev.* **1999**, *99*, 1787–1800. [CrossRef]
94. Bilal, M.; Shah, J.A.; Ashfaq, T.; Gardazi, S.M.H.; Tahir, A.A.; Pervez, A.; Haroon, H.; Mahmood, Q. Waste biomass adsorbents for copper removal from industrial wastewater—A review. *J. Hazard. Mater.* **2013**, *263*, 322–333. [CrossRef]
95. Danish, M.; Ahmad, T. A review on utilization of wood biomass as a sustainable precursor for activated carbon production and application. *Renew. Sustain. Energy Rev.* **2018**, *87*, 1–21. [CrossRef]
96. Jain, A.; Balasubramanian, R.; Srinivasan, M.P. Hydrothermal conversion of biomass waste to activated carbon with high porosity: A review. *Chem. Eng. J.* **2016**, *283*, 789–805. [CrossRef]
97. Mohamad Nor, N.; Lau, L.C.; Lee, K.T.; Mohamed, A.R. Synthesis of activated carbon from lignocellulosic biomass and its applications in air pollution control—A review. *J. Environ. Chem. Eng.* **2013**, *1*, 658–666. [CrossRef]
98. Wang, J.; Kaskel, S. KOH activation of carbon-based materials for energy storage. *J. Mater. Chem.* **2012**, *22*, 23710–23725. [CrossRef]
99. Anićijević, V.J.; Lazarević-Pašti, T.D.; Vasić, V.M.; Vasić Anićijević, D.D. An Insight into the Efficient Dimethoate Adsorption on Graphene-Based Materials—A Combined Experimental and DFT Study. *Appl. Sci.* **2021**, *11*, 4014. [CrossRef]
100. Anićijević, V.; Jelić, M.; Jovanović, A.Z.; Potkonjak, N.; Pašti, I.A.; Lazarević Pašti, T.D. Organophosphorous pesticide removal from water by graphene-based materials—Only adsorption or something else as well? *J. Serbian Chem. Soc.* **2021**, *86*, 699–710. [CrossRef]
101. Jing, L.; Li, P.; Li, Z.; Ma, D.; Hu, J. Influence of π-π interactions on organic photocatalytic materials and their performance. *Chem. Soc. Rev.* **2025**, *54*, 2054–2090. [CrossRef]
102. Pérez, E.M.; Martín, N. π-π interactions in carbon nanostructures. *Chem. Soc. Rev.* **2015**, *44*, 6425–6433. [CrossRef] [PubMed]

103. Georgakilas, V.; Tiwari, J.N.; Kemp, K.C.; Perman, J.A.; Bourlinos, A.B.; Kim, K.S.; Zboril, R. Noncovalent Functionalization of Graphene and Graphene Oxide for Energy Materials, Biosensing, Catalytic, and Biomedical Applications. *Chem. Rev.* **2016**, *116*, 5464–5519. [CrossRef] [PubMed]
104. Santos, Y.H.; Martinez, A.H.G.; Veiga, A.G.; Rocco, M.L.M.; Zarbin, A.J.G.; Orth, E.S. Site-selective Mono- and Bifunctionalization of Graphene Oxide: Screening Nanocatalysts for Organophosphate Degradation. *ChemCatChem* **2024**, *16*, e202301440. [CrossRef]
105. Santos, Y.; Hostert, L.; Almeida, T.; Zarbin, A.; Souza, V.; Orth, E. Functionalized Crumpled Graphene as Nanocatalysts for Organophosphate Neutralization. *J. Braz. Chem. Soc.* **2024**, *35*, e-20240063. [CrossRef]
106. Suo, F.; Xie, G.; Zhang, J.; Li, J.; Li, C.; Liu, X.; Zhang, Y.; Ma, Y.; Ji, M. A carbonised sieve-like corn straw cellulose–graphene oxide composite for organophosphorus pesticide removal. *RSC Adv.* **2018**, *8*, 7735–7743. [CrossRef]
107. Rahman, A.J.; Ojha, H.; Pandey, A.; Kumar, S.; Singhal, R.; Datta, A.; Singh, B.K. Kinetic, isotherm and thermodynamic adsorption studies of organophosphorus compound (phosmet) on reduced graphene oxide. *Diam. Relat. Mater.* **2022**, *127*, 109191. [CrossRef]
108. Hou, X.; Yu, H.; Zhu, F.; Li, Z.; Yang, Q. Determination of organophosphorus pesticides based on graphene oxide aerogel solid phase extraction column. *Se Pu Chin. J. Chromatogr.* **2022**, *40*, 10–16. [CrossRef] [PubMed]
109. Sahu, D.; Pervez, S.; Karbhal, I.; Tamrakar, A.; Mishra, A.; Verma, S.R.; Deb, M.K.; Ghosh, K.K.; Pervez, Y.F.; Shrivas, K.; et al. Applications of different adsorbent materials for the removal of organic and inorganic contaminants from water and wastewater—A review. *Desalination Water Treat.* **2024**, *317*, 100253. [CrossRef]
110. Pasti, I.; Breitenbach, S.; Unterweger, C.; Fuerst, C. *Carbon Materials as Adsorbents for Organophosphate Pesticides in Aqueous Media—Critical Overview*; Nova Science Publishers: New York, NY, USA, 2022; p. 251. Available online: https://www.scopus.com/pages/publications/85138978704?origin=resultslist (accessed on 25 September 2025).
111. Wanjeri, V.W.O.; Sheppard, C.J.; Prinsloo, A.R.E.; Ngila, J.C.; Ndungu, P.G. Isotherm and kinetic investigations on the adsorption of organophosphorus pesticides on graphene oxide based silica coated magnetic nanoparticles functionalized with 2-phenylethylamine. *J. Environ. Chem. Eng.* **2018**, *6*, 1333–1346. [CrossRef]
112. Yadav, S.; Goel, N.; Kumar, V.; Singhal, S. Graphene Oxide as Proficient Adsorbent for the Removal of Harmful Pesticides: Comprehensive Experimental Cum DFT Investigations. *Anal. Chem. Lett.* **2019**, *9*, 291–310. [CrossRef]
113. Han, Q.; Yang, L.; Liang, Q.; Ding, M. Three-dimensional hierarchical porous graphene aerogel for efficient adsorption and preconcentration of chemical warfare agents. *Carbon* **2017**, *122*, 556–563. [CrossRef]
114. Nikou, M.; Samadi-Maybodi, A.; Yasrebi, K.; Sedighi-Pashaki, E. Simultaneous monitoring of the adsorption process of two organophosphorus pesticides by employing GO/ZIF-8 composite as an adsorbent. *Environ. Technol. Innov.* **2021**, *23*, 101590. [CrossRef]
115. Nasiri, M.; Ahmadzadeh, H.; Amiri, A. Organophosphorus pesticides extraction with polyvinyl alcohol coated magnetic graphene oxide particles and analysis by gas chromatography-mass spectrometry: Application to apple juice and environmental water. *Talanta* **2021**, *227*, 122078. [CrossRef]
116. Sohrabi, N.; Mohammadi, R.; Ghassemzadeh, H.R.; Heris, S.S.S. Equilibrium, kinetic and thermodynamic study of diazinon adsorption from water by clay/GO/Fe_3O_4: Modeling and optimization based on response surface methodology and artificial neural network. *J. Mol. Liq.* **2021**, *328*, 115384. [CrossRef]
117. Dolatabadi, M.; Naidu, H.; Ahmadzadeh, S. Adsorption characteristics in the removal of chlorpyrifos from groundwater using magnetic graphene oxide and carboxy methyl cellulose composite. *Sep. Purif. Technol.* **2022**, *300*, 121919. [CrossRef]
118. Perović, M.; Obradović, V.; Zuber-Radenković, V.; Mitrinović, D.; Knoeller, K.; Turk Sekulić, M. Integrated analysis of ammonium origins in a Serbian anoxic alluvial aquifer: Insight from physicochemical, isotopic, microbiological data. *Appl. Geochem.* **2024**, *171*, 106103. [CrossRef]
119. Perović, M.; Obradović, V.; Zuber-Radenković, V.; Knoeller, K.; Mitrinović, D.; Čepić, Z. The comprehensive evaluation of nitrate origin and transformation pathways in the oxic alluvial aquifer in Serbia. *Environ. Sci. Pollut. Res.* **2024**, *31*, 33030–33046. [CrossRef]
120. Živančev, N.; Kovačević, S.; Perović, M.; Čalenić, A.; Dimkić, M. Influence of oxic and anoxic groundwater conditions on occurrence of selected agrochemicals. *Water Supply* **2019**, *20*, 487–498. [CrossRef]
121. Morguen, M.; Rach, A.; Colbeau-Justin, C.; Robert, D.; Keller, V. Self-Decontaminating Photocatalytic Textiles: Layer-by-Layer Deposition of Commercial TiO_2 References for DMMP Degradation. *ACS Appl. Eng. Mater.* **2025**, *3*, 1995–2006. [CrossRef]
122. Henych, J.; Štengl, V.; Mattsson, A.; Tolasz, J.; Österlund, L. Chemical warfare agent simulant DMMP reactive adsorption on TiO_2/graphene oxide composites prepared via titanium peroxo-complex or urea precipitation. *J. Hazard. Mater.* **2018**, *359*, 482–490. [CrossRef]
123. Kumar, R.; George, L.; Jun, Z.; Mukherji, S. Photocatalytic activity of graphene oxide-TiO_2 nanocomposite on dichlorvos and malathion and assessment of toxicity changes due to photodegradation. *Chemosphere* **2022**, *308*, 136402. [CrossRef]
124. Kumar, R.; Mukherji, S. Photocatalysis of dichlorvos using graphene oxide-TiO_2 nanocomposite under visible irradiation: Process optimization using response surface methodology. *Nanotechnology* **2021**, *32*, 405708. [CrossRef] [PubMed]

125. Kumar, R.; Mukherji, S. Assessment of Photocatalytic Efficiency of Graphene Oxide–TiO_2 Nanocomposite for Removal of Binary Mixtures of Organophosphorus Pesticides from Water. *ACS EST Water* **2024**, *4*, 4075–4082. [CrossRef]
126. Giannakoudakis, D.A.; Farahmand, N.; Łomot, D.; Sobczak, K.; Bandosz, T.J.; Colmenares, J.C. Ultrasound-activated TiO_2/GO-based bifunctional photoreactive adsorbents for detoxification of chemical warfare agent surrogate vapors. *Chem. Eng. J.* **2020**, *395*, 125099. [CrossRef]
127. Martínez-Perales, C.; Machín, A.; Berríos-Rolón, P.J.; Sampayo, P.; Nieves, E.; Soto-Vázquez, L.; Resto, E.; Morant, C.; Ducongé, J.; Cotto, M.C.; et al. From Pollutant Removal to Renewable Energy: MoS_2-Enhanced P25-Graphene Photocatalysts for Malathion Degradation and H_2 Evolution. *Materials* **2025**, *18*, 2602. [CrossRef] [PubMed]
128. Uyen, N.N.; Tu, L.A.; Le, P.H. Graphene quantum dot-decorated TiO_2 nanowires/nanotubes: Enhanced photocatalysis for methylene blue and pesticide degradation. *Appl. Phys. A* **2025**, *131*, 302. [CrossRef]
129. Mohamed, R.M. UV-assisted photocatalytic synthesis of TiO_2-reduced graphene oxide with enhanced photocatalytic activity in decomposition of sarin in gas phase. *Desalination Water Treat.* **2012**, *50*, 147–156. [CrossRef]
130. Sumantrao, S.K.; Kariyajjanavar, P.; Vidyasagar, C.C.; Shridhar, A.H.; Ghagane, S.C.; Chigari, S.S.; Bonageri, G.; Ansari, M.Z.; Alsubaie, A.S. Sunlight-driven GO/ZnO nanocomposite for photocatalytic degradation of Chlorpyrifos insecticide and its biological activities. *J. Environ. Chem. Eng.* **2025**, *13*, 115437. [CrossRef]
131. Zhu, Z.; Guo, F.; Xu, Z.; Di, X.; Zhang, Q. Photocatalytic degradation of an organophosphorus pesticide using a ZnO/rGO composite. *RSC Adv.* **2020**, *10*, 11929–11938. [CrossRef] [PubMed]
132. Mohammadi, A.; Mirhosseini, H.; Hekmatiyan, A.; Abdolahi, L.; Mehrabi, F.; Shahmirzaei, M. Efficient degradation of parathion as a pollutant and diazinon as a nerve agent by reaction mechanism with rGO-Co_3O_4/ZnO nanocomposite photocatalyst. *J. Environ. Chem. Eng.* **2023**, *11*, 110912. [CrossRef]
133. Pirsaheb, M.; Hossaini, H.; Fatahi, N.; Jafari, Z.; Jafari, F.; Jafari Motlagh, R. Photocatalytic removal of organophosphorus pesticide by the WO_3-Fe_3O_4/rGO photocatalyst under visible light. *Environ. Sci. Pollut. Res.* **2024**, *31*, 2555–2568. [CrossRef]
134. Tabasum, S.; Rani, S.; Sharma, A.; Dhupar, N.; Singh, P.P.; Bagri, U.; Kumar, D. Efficient Photocatalytic Degradation of Chlorpyrifos Pesticide from Aquatic Agricultural Waste Using g-C_3N_4 Decorated Graphene Oxide/V_2O_5 Nanocomposite. *Top. Catal.* **2024**, *67*, 725–736. [CrossRef]
135. Naynava, S.K.; Lorestani, B.; Cheraghi, M.; Sobhanardakani, S.; Shahmoradi, B. Efficient Degradation of Diazinon Pesticide under Visible Light Irradiation Using CeO_2 Functionalized Magnetite Graphene Oxide Heterojunction-Based Photocatalyst. *Water Air Soil Pollut.* **2024**, *235*, 274. [CrossRef]
136. Samy, M.; Ibrahim, M.G.; Gar Alalm, M.; Fujii, M.; Diab, K.E.; ElKady, M. Innovative photocatalytic reactor for the degradation of chlorpyrifos using a coated composite of ZrV_2O_7 and graphene nano-platelets. *Chem. Eng. J.* **2020**, *395*, 124974. [CrossRef]
137. Saljooqi, A.; Shamspur, T.; Mostafavi, A. Synthesis of titanium nanoplate decorated by Pd and Fe_3O_4 nanoparticles immobilized on graphene oxide as a novel photocatalyst for degradation of parathion pesticide. *Polyhedron* **2020**, *179*, 114371. [CrossRef]
138. Fakhri, H.; Farzadkia, M.; Boukherroub, R.; Srivastava, V.; Sillanpää, M. Design and preparation of core-shell structured magnetic graphene oxide@MIL-101(Fe): Photocatalysis under shell to remove diazinon and atrazine pesticides. *Sol. Energy* **2020**, *208*, 990–1000. [CrossRef]
139. Chinnappa, K.; Karuna Ananthai, P.; Srinivasan, P.P.; Dharmaraj Glorybai, C. Green synthesis of rGO-AgNP composite using Curcubita maxima extract for enhanced photocatalytic degradation of the organophosphate pesticide chlorpyrifos. *Environ. Sci. Pollut. Res. Int.* **2022**, *29*, 58121–58132. [CrossRef]
140. Henych, J.; Mattsson, A.; Tolasz, J.; Štengl, V.; Österlund, L. Solar light decomposition of warfare agent simulant DMMP on TiO_2/graphene oxide nanocomposites. *Catal. Sci. Technol.* **2019**, *9*, 1816–1824. [CrossRef]
141. Dipak, P.; Gahlaut, U.P.S.; Goswami, Y.C. Visible light photocatalytic reduction of toxic chemical organophosphate monocrotophos using reduced graphene oxide derived from bamboo leaves. *Sustain. Chem. One World* **2024**, *4*, 100031. [CrossRef]
142. Pirsaheb, M.; Hossaini, H.; Asadi, A.; Jafari, Z. Persulfate activation by magnetic SnS_2-Fe_3O_4/rGO nanocomposite under visible light for detoxification of organophosphorus pesticide. *J. Mol. Liq.* **2022**, *364*, 119975. [CrossRef]
143. Zangiabadi, M.; Shamspur, T.; Saljooqi, A.; Mostafavi, A. Evaluating the efficiency of the GO-Fe_3O_4/TiO_2 mesoporous photocatalyst for degradation of chlorpyrifos pesticide under visible light irradiation. *Appl. Organomet. Chem.* **2019**, *33*, e4813. [CrossRef]
144. Gupta, V.K.; Eren, T.; Atar, N.; Yola, M.L.; Parlak, C.; Karimi-Maleh, H. $CoFe_2O_4$@TiO_2 decorated reduced graphene oxide nanocomposite for photocatalytic degradation of chlorpyrifos. *J. Mol. Liq.* **2015**, *208*, 122–129. [CrossRef]
145. Mohammadi, M.; Maleki, A.; Zandi, S.; Mohammadi, E.; Ghahremani, E.; Yang, J.-K.; Lee, S.-M. Photocatalytic decomposition of aqueous diazinon using reduced graphene/ZnO nanocomposite doped with manganese. *Desalination Water Treat.* **2020**, *184*, 315–325. [CrossRef]
146. Kong, E.D.H.; Chau, J.H.F.; Lai, C.W.; Khe, C.S.; Sharma, G.; Kumar, A.; Siengchin, S.; Sanjay, M.R. GO/TiO_2-Related Nanocomposites as Photocatalysts for Pollutant Removal in Wastewater Treatment. *Nanomaterials* **2022**, *12*, 3536. [CrossRef] [PubMed]

147. Nasir, A.; Khalid, S.; Yasin, T.; Mazare, A. A Review on the Progress and Future of TiO_2/Graphene Photocatalysts. *Energies* **2022**, *15*, 6248. [CrossRef]
148. Zhang, L.; Du, L.; Yu, X.; Tan, S.; Cai, X.; Yang, P.; Gu, Y.; Mai, W. Significantly enhanced photocatalytic activities and charge separation mechanism of Pd-decorated ZnO-graphene oxide nanocomposites. *ACS Appl. Mater. Interfaces* **2014**, *6*, 3623–3629. [CrossRef]
149. Yu, T.; Breslin, C.B. Graphene-Modified Composites and Electrodes and Their Potential Applications in the Electro-Fenton Process. *Materials* **2020**, *13*, 2254. [CrossRef]
150. Jia, J.; Li, Z.; Tian, Y.; Li, X.; Chen, R.; Liu, J.; Liang, J. Electrosynthesis of H_2O_2 via two-electron oxygen reduction over carbon-based catalysts: From microenvironment control to electrode/reactor design. *Energy Rev.* **2024**, *3*, 100069. [CrossRef]
151. Ozturk, D. Fe_3O_4/Mn_3O_4/ZnO-rGO hybrid quaternary nano-catalyst for effective treatment of tannery wastewater with the heterogeneous electro-Fenton process: Process optimization. *Sci. Total Environ.* **2022**, *828*, 154473. [CrossRef]
152. Huang, L.; Zhao, Y.; Bai, Y.; Song, J.; Sun, G. Recent Advances in the Electron Transfer Mechanism of Fe-Based Electro-Fenton Catalysts for Emerging Organic Contaminant Degradation. *Catalysts* **2025**, *15*, 549. [CrossRef]
153. Sankar, M.; He, Q.; Engel, R.V.; Sainna, M.A.; Logsdail, A.J.; Roldan, A.; Willock, D.J.; Agarwal, N.; Kiely, C.J.; Hutchings, G.J. Role of the Support in Gold-Containing Nanoparticles as Heterogeneous Catalysts. *Chem. Rev.* **2020**, *120*, 3890–3938. [CrossRef]
154. Senthilnathan, J.; Younis, S.A.; Kwon, E.E.; Surenjan, A.; Kim, K.-H.; Yoshimura, M. An efficient system for electro-Fenton oxidation of pesticide by a reduced graphene oxide-aminopyrazine@3DNi foam gas diffusion electrode. *J. Hazard. Mater.* **2020**, *400*, 123323. [CrossRef]
155. Chai, D.; Chen, Y.; Jiang, Z.; Li, Z.; Zhang, X.; Chen, X.; Wang, Y.; Cui, K. Insight on magnetic nitrogen-doped graphene oxide composite electrode constructing heterogeneous Electro-Fenton system for treating organophosphorus pesticide wastewater. *Sep. Purif. Technol.* **2024**, *345*, 127419. [CrossRef]
156. Ayoubi-Feiz, B.; Mashhadizadeh, M.H.; Sheydaei, M. Degradation of diazinon by new hybrid nanocomposites N-TiO_2/Graphene/Au and N-TiO_2/Graphene/Ag using visible light photo-electro catalysis and photo-electro catalytic ozonation: Optimization and comparative study by Taguchi method. *Sep. Purif. Technol.* **2019**, *211*, 704–714. [CrossRef]
157. Yadav, P.; Sharma, P.; Roy, T.; Kumar, A.; Kumar, D.; Mudila, H.; Kumar, S.P.; Ghotekar, S.; Mubarak, N.M.; Hosseini-Bandegharaei, A.; et al. Exploring catalytic applications of graphene-transition metal oxide nanocomposites for next-generation catalysis: A review. *Inorg. Chem. Commun.* **2025**, *178*, 114506. [CrossRef]
158. Ambrosi, A.; Chua, C.K.; Bonanni, A.; Pumera, M. Electrochemistry of Graphene and Related Materials. *Chem. Rev.* **2014**, *114*, 7150–7188. [CrossRef]
159. Lumbaque, E.C.; Radjenovic, J. Electro-oxidation of persistent organic contaminants at graphene sponge electrodes using intermittent current. *Chem. Eng. J.* **2023**, *476*, 146910. [CrossRef]
160. Mohd Razib, M.S.; Latip, W.; Abdul Rashid, J.I.; Knight, V.F.; Wan Yunus, W.M.Z.; Ong, K.K.; Mohd Kasim, N.A.; Mohd Noor, S.A. An Enzyme-Based Biosensor for the Detection of Organophosphate Compounds Using Mutant Phosphotriesterase Immobilized onto Reduced Graphene Oxide. *J. Chem.* **2021**, *2021*, 2231089. [CrossRef]
161. Chen, J.; Guo, Z.; Xin, Y.; Gu, Z.; Zhang, L.; Guo, X. Effective remediation and decontamination of organophosphorus compounds using enzymes: From rational design to potential applications. *Sci. Total Environ.* **2023**, *867*, 161510. [CrossRef]
162. Chen, Y.; Luo, Z.; Lu, X. Construction of Novel Enzyme–Graphene Oxide Catalytic Interface with Improved Enzymatic Performance and Its Assembly Mechanism. *ACS Appl. Mater. Interfaces* **2019**, *11*, 11349–11359. [CrossRef]
163. Ma, X.; Zhang, L.; Xia, M.; Li, S.; Zhang, X.; Zhang, Y. Mimicking the Active Sites of Organophosphorus Hydrolase on the Backbone of Graphene Oxide to Destroy Nerve Agent Simulants. *ACS Appl. Mater. Interfaces* **2017**, *9*, 21089–21093. [CrossRef] [PubMed]
164. Ma, X.; Zhang, L.; Xia, M.; Zhang, X.; Zhang, Y. Catalytic degradation of organophosphorous nerve agent simulants by polymer beads@graphene oxide with organophosphorus hydrolase-like activity based on rational design of functional bimetallic nuclear ligand. *J. Hazard. Mater.* **2018**, *355*, 65–73. [CrossRef] [PubMed]
165. Hamid, F.H.; Rasyid, F.R.; Mashuni, M.; Ahmad, L.O.; Jahiding, M. Enhanced rGO/ZnO/Chitosan Nanozyme Photocatalytic Technology for Efficient Degradation of Diazinon Pesticide Contaminated Water. *Adsorption* **2024**, *31*, 22. [CrossRef]
166. Alexandre, A.d.C.; Letícia, C.A.; Daniela, R.S.; Silviana, C.; Tamiris, M.A.; Giovanna, C.G.; Flávia, V.S.; Teodorico, C.R. Computational enzymology for degradation of chemical warfare agents: Promising technologies for remediation processes. *AIMS Microbiol.* **2017**, *3*, 108–135. [CrossRef]
167. Khoj, M.A.; Awwad, N.S.; Ibrahium, H.A.; Awad, A.M.; Hassan, A.F. Enhanced Adsorption and Photo-Fenton Degradation of Diazinon Pesticide Utilizing Nanomagnetite/Graphene Oxide Composite: Kinetic and Thermodynamic Studies. *J. Inorg. Organomet. Polym. Mater.* **2024**, *34*, 3483–3500. [CrossRef]
168. Dolatabadi, M.; Świergosz, T.; Wang, C.; Ahmadzadeh, S. Accelerated degradation of groundwater-containing malathion using persulfate activated magnetic Fe3O4/graphene oxide nanocomposite for advanced water treatment. *Arab. J. Chem.* **2023**, *16*, 104424. [CrossRef]

169. Arfaeinia, H.; Rezaei, H.; Sharafi, K.; Moradi, M.; Pasalari, H.; Hashemi, S.E. Application of ozone/magnetic graphene oxide for degradation of diazinon pesticide from aqueous solutions. *Desalination Water Treat.* **2018**, *107*, 127–135. [CrossRef]
170. Assafi, A.; Zarouki, M.A.; Hejji, L.; Aoulad El Hadj Ali, Y.; Chraka, A.; Pérez-Villarejo, L.; Sánchez-Soto, P.J.; Souhail, B.; Azzouz, A. Olive pomace-derived graphene quantum dots decorated with iron oxide nanoparticles for efficient malathion removal from environmental water: Theoretical and experimental studies. *Diam. Relat. Mater.* **2025**, *155*, 112255. [CrossRef]
171. Cao, S.; Zhou, Y.; Xi, C.; Tang, T.; Chen, Z. Enhanced adsorption of malathion and phoxim by a three-dimensional magnetic graphene oxide-functionalized citrus peel-derived bio-composite. *Anal. Methods* **2021**, *13*, 2951–2962. [CrossRef] [PubMed]
172. Barzegarzadeh, M.; Amini-Fazl, M.S.; Sohrabi, N. Ultrasound-assisted adsorption of chlorpyrifos from aqueous solutions using magnetic chitosan/graphene quantum dot-iron oxide nanocomposite hydrogel beads in batch adsorption column and fixed bed. *Int. J. Biol. Macromol.* **2023**, *242*, 124587. [CrossRef]
173. Rahmatpour, A.; Hesarsorkh, A.H.A. Self-assembly of graphene oxide containing bio-nanocomposite hydrogels for removal of chlorpyrifos and methylene blue. *Int. J. Biol. Macromol.* **2025**, *320*, 145850. [CrossRef] [PubMed]
174. Alipoori, S.; Rouhi, H.; Linn, E.; Stumpfl, H.; Mokarizadeh, H.; Esfahani, M.R.; Koh, A.; Weinman, S.T.; Wujcik, E.K. Polymer-Based Devices and Remediation Strategies for Emerging Contaminants in Water. *ACS Appl. Polym. Mater.* **2021**, *3*, 549–577. [CrossRef]
175. Song, L.; Zhao, T.; Yang, D.; Wang, X.; Hao, X.; Liu, Y.; Zhang, S.; Yu, Z.-Z. Photothermal graphene/UiO-66-NH_2 fabrics for ultrafast catalytic degradation of chemical warfare agent simulants. *J. Hazard. Mater.* **2020**, *393*, 122332. [CrossRef]
176. Najafi, A.; Maddah, B.; Fakhraian, H. The effect of adding carbon nanotubes to 3D graphene on the adsorption of DMMP from airflow. *Diam. Relat. Mater.* **2024**, *142*, 110806. [CrossRef]
177. Šťastný, M.; Tolasz, J.; Štengl, V.; Henych, J.; Žižka, D. Graphene oxide/MnO_2 nanocomposite as destructive adsorbent of nerve-agent simulants in aqueous media. *Appl. Surf. Sci.* **2017**, *412*, 19–28. [CrossRef]
178. Arcibar-Orozco, J.A.; Giannakoudakis, D.A.; Bandosz, T.J. Copper Hydroxyl Nitrate/Graphite Oxide Composite as Superoxidant for the Decomposition/Mineralization of Organophosphate-Based Chemical Warfare Agent Surrogate. *Adv. Mater. Interfaces* **2015**, *2*, 1500215. [CrossRef]
179. Jang, S.; Ka, D.; Jung, H.; Kim, M.-K.; Jung, H.; Jin, Y. $Zr(OH)_4$/GO Nanocomposite for the Degradation of Nerve Agent Soman (GD) in High-Humidity Environments. *Materials* **2020**, *13*, 2954. [CrossRef] [PubMed]
180. Yang, Q.; Lu, L.; Xu, Q.; Tang, S.; Yu, Y. Using Post-graphene 2D Materials to Detect and Remove Pesticides: Recent Advances and Future Recommendations. *Bull. Environ. Contam. Toxicol.* **2021**, *107*, 185–193. [CrossRef]
181. Silva, V.B.; Santos, Y.H.; Hellinger, R.; Mansour, S.; Delaune, A.; Legros, J.; Zinoviev, S.; Nogueira, E.S.; Orth, E.S. Organophosphorus chemical security from a peaceful perspective: Sustainable practices in its synthesis, decontamination and detection. *Green Chem.* **2022**, *24*, 585–613. [CrossRef]
182. Hassanzadeh-Afruzi, F.; Esmailzadeh, F.; Taheri-Ledari, R.; Maleki, A. High adsorption capability of chlorpyrifos and Congo red in aqueous samples by a functionalized dextrin/graphene oxide composite. *Int. J. Environ. Sci. Technol.* **2023**, *20*, 10731–10750. [CrossRef]
183. Kamel, A.H.; Abd-Rabboh, H.S.M.; Abd El-Fattah, A.; Boudghene Stambouli, G.; Adeida, L. Metal oxides and their composites for the remediation of organic pesticides: Advanced photocatalytic and adsorptive solutions. *RSC Adv.* **2025**, *15*, 6875–6901. [CrossRef]
184. Aziz, K.; Naz, A.; Raza, N.; Manzoor, S.; Kim, K.-H. Reduced and modified graphene oxide with Ag/V_2O_5 as a ternary composite visible light photocatalyst against dyes and pesticides. *Environ. Res.* **2024**, *247*, 118256. [CrossRef]
185. Wu, L.; Liu, L.; Gao, B.; Muñoz-Carpena, R.; Zhang, M.; Chen, H.; Zhou, Z.; Wang, H. Aggregation Kinetics of Graphene Oxides in Aqueous Solutions: Experiments, Mechanisms, and Modeling. *Langmuir* **2013**, *29*, 15174–15181. [CrossRef]
186. Liu, L.; Liu, S.; Zhang, Q.; Li, C.; Bao, C.; Liu, X.; Xiao, P. Adsorption of Au(III), Pd(II), and Pt(IV) from Aqueous Solution onto Graphene Oxide. *J. Chem. Eng. Data* **2013**, *58*, 209–216. [CrossRef]
187. Chen, X.; Zhou, S.; Zhang, L.; You, T.; Xu, F. Adsorption of Heavy Metals by Graphene Oxide/Cellulose Hydrogel Prepared from NaOH/Urea Aqueous Solution. *Materials* **2016**, *9*, 582. [CrossRef]
188. Nirmala, N.; Shriniti, V.; Aasresha, K.; Arun, J.; Gopinath, K.P.; Dawn, S.S.; Sheeladevi, A.; Priyadharsini, P.; Birindhadevi, K.; Chi, N.T.L.; et al. Removal of toxic metals from wastewater environment by graphene-based composites: A review on isotherm and kinetic models, recent trends, challenges and future directions. *Sci. Total Environ.* **2022**, *840*, 156564. [CrossRef]
189. Singh, S.; Naik, T.S.S.K.; Shehata, N.; Aguilar-Marcelino, L.; Dhokne, K.; Lonare, S.; Chauhan, V.; Kumar, A.; Singh, J.; Ramamurthy, P.C.; et al. Novel insights into graphene oxide-based adsorbents for remediation of hazardous pollutants from aqueous solutions: A comprehensive review. *J. Mol. Liq.* **2023**, *369*, 120821. [CrossRef]
190. Gong, Y.; Yu, Y.; Kang, H.; Chen, X.; Liu, H.; Zhang, Y.; Sun, Y.; Song, H. Synthesis and Characterization of Graphene Oxide/Chitosan Composite Aerogels with High Mechanical Performance. *Polymers* **2019**, *11*, 777. [CrossRef]
191. Pinelli, F.; Nespoli, T.; Rossi, F. Graphene Oxide-Chitosan Aerogels: Synthesis, Characterization, and Use as Adsorbent Material for Water Contaminants. *Gels* **2021**, *7*, 149. [CrossRef]

192. Yang, J.; Guo, S.; Dong, H.; Liu, Y.; Wang, J.; Quan, G.; Zhang, X.; Lei, J.; Liu, N. Enhanced visible-light-driven photocatalysis of ibuprofen by NH2 modified MIL-53(Fe) graphene aerogel: Performance, mechanism, pathway and toxicity assessment. *Colloids Surf. A Physicochem. Eng. Asp.* **2025**, *726*, 137769. [CrossRef]
193. Chhetri, S.; Kuila, T. Polymer composites with 3D graphene architectures as high-performance EMI shielding materials: A review. *RSC Appl. Polym.* **2024**, *2*, 507–533. [CrossRef]
194. Chowdhury, I.; Duch, M.C.; Mansukhani, N.D.; Hersam, M.C.; Bouchard, D. Colloidal Properties and Stability of Graphene Oxide Nanomaterials in the Aquatic Environment. *Environ. Sci. Technol.* **2013**, *47*, 6288–6296. [CrossRef]
195. Ahmed, F.; Rodrigues, D.F. Investigation of acute effects of graphene oxide on wastewater microbial community: A case study. *J. Hazard. Mater.* **2013**, *256–257*, 33–39. [CrossRef] [PubMed]
196. Jyothi, B.A.; Sri, A.S.; Bhuvaneshwari, K.; Sravani, A.J.; Madhavi, V. A comprehensive emphasis on graphene technology and its bioscience applications. *Sustain. Chem. One World* **2025**, *6*, 100063. [CrossRef]
197. Safian, M.T.-u.; Umar, K.; Mohamad Ibrahim, M.N. Synthesis and scalability of graphene and its derivatives: A journey towards sustainable and commercial material. *J. Clean. Prod.* **2021**, *318*, 128603. [CrossRef]
198. Johnson, R.; Zafar, M.A.; Thomas, S.; Jacob, M.V. A critical review on vacuum and atmospheric microwave plasma-based graphene synthesis. *FlatChem* **2025**, *50*, 100812. [CrossRef]
199. Syama, S.; Mohanan, P.V. Safety and biocompatibility of graphene: A new generation nanomaterial for biomedical application. *Int. J. Biol. Macromol.* **2016**, *86*, 546–555. [CrossRef]
200. Abuzeyad, O.H.; El-Khawaga, A.M.; Tantawy, H.; Elsayed, M.A. An evaluation of the improved catalytic performance of rGO/GO-hybrid-nanomaterials in photocatalytic degradation and antibacterial activity processes for wastewater treatment: A review. *J. Mol. Struct.* **2023**, *1288*, 135787. [CrossRef]
201. Nguyen, H.N.; Rodrigues, D.F. Chronic toxicity of graphene and graphene oxide in sequencing batch bioreactors: A comparative investigation. *J. Hazard. Mater.* **2018**, *343*, 200–207. [CrossRef]
202. Zhao, J.; Wang, Z.; White, J.C.; Xing, B. Graphene in the Aquatic Environment: Adsorption, Dispersion, Toxicity and Transformation. *Environ. Sci. Technol.* **2014**, *48*, 9995–10009. [CrossRef]
203. Chang, Y.; Yang, S.-T.; Liu, J.-H.; Dong, E.; Wang, Y.; Cao, A.; Liu, Y.; Wang, H. In vitro toxicity evaluation of graphene oxide on A549 cells. *Toxicol. Lett.* **2011**, *200*, 201–210. [CrossRef] [PubMed]
204. Jia, P.-P.; Sun, T.; Junaid, M.; Yang, L.; Ma, Y.-B.; Cui, Z.-S.; Wei, D.-P.; Shi, H.-F.; Pei, D.-S. Nanotoxicity of different sizes of graphene (G) and graphene oxide (GO) in vitro and in vivo. *Environ. Pollut.* **2019**, *247*, 595–606. [CrossRef]
205. Sundar, L.S.; Ashraf, M.W. Synthesis and characterization methods of graphene oxide nanomaterial for biomedical and toxicity applications: A comprehensive review. *Inorg. Chem. Commun.* **2025**, *174*, 113936. [CrossRef]
206. Krishnaraj, C.; Kaliannagounder, V.K.; Rajan, R.; Ramesh, T.; Kim, C.S.; Park, C.H.; Liu, B.; Yun, S.-I. Silver nanoparticles decorated reduced graphene oxide: Eco-friendly synthesis, characterization, biological activities and embryo toxicity studies. *Environ. Res.* **2022**, *210*, 112864. [CrossRef]
207. Tewari, C.; Tatrari, G.; Kumar, S.; Pandey, S.; Rana, A.; Pal, M.; Sahoo, N.G. Green and cost-effective synthesis of 2D and 3D graphene-based nanomaterials from Drepanostachyum falcatum for bio-imaging and water purification applications. *Chem. Eng. J. Adv.* **2022**, *10*, 100265. [CrossRef]

Disclaimer/Publisher's Note: The statements, opinions and data contained in all publications are solely those of the individual author(s) and contributor(s) and not of MDPI and/or the editor(s). MDPI and/or the editor(s) disclaim responsibility for any injury to people or property resulting from any ideas, methods, instructions or products referred to in the content.